Miner Deposita (2008) 43:805–824
DOI 10.1007/s00126-008-0197-z

ARTICLE

Geology, fluid inclusion and sulphur isotope characteristics of the El Cobre VHMS deposit, Southern Cuba

Xiomara Cazañas · Pura Alfonso · Joan Carles Melgarejo · Joaquín Antonio Proenza · Anthony Edward Fallick

Received: 26 January 2006 / Accepted: 27 May 2008 / Published online: 28 June 2008

Abstract The El Cobre deposit is located in eastern Cuba within the volcanosedimentary sequence of the Sierra Maestra Paleogene arc. The deposit is hosted by tholeiitic basalts, andesites and tuffs and comprises thick stratiform barite and anhydrite bodies, three stratabound disseminated up to massive sulphide bodies produced by silicification and sulphidation of limestones or sulphates, an anhydrite stockwork and a siliceous stockwork, grading downwards to quartz veins. Sulphides are mainly pyrite, chalcopyrite and sphalerite; gold occurs in the stratabound ores. Fluid inclusions measured in sphalerite, quartz, anhydrite and calcite show salinities between 2.3 and 5.7 wt% NaCl eq. and homogenisation temperatures between 177 and 300°C. Sulphides from the stratabound mineralisation display δ^{34}S values of 0‰ to +6.0‰, whilst those from the feeder zone lie between −1.4‰ and +7.3‰. Sulphides show an intra-grain sulphur isotope zonation of about 2‰; usually, δ^{34}S values increase towards the rims. Sulphate sulphur has δ^{34}S in the range of +17‰ to +21‰, except two samples with values of +5.9‰ and +7.7‰. Sulphur isotope data indicate that the thermochemical reduction of sulphate from a hydrothermal fluid of seawater origin was the main source of sulphide sulphur and that most of the sulphates precipitated by heating of seawater. The structure of the deposit, mineralogy, fluid inclusion and isotope data suggest that the deposit formed from seawater-derived fluids with probably minor supply of magmatic fluids.

Keywords VHMS deposit · Sulphides · Fluid inclusions · S isotopes · Cuba

Editorial handling: A. Boyce

X. Cazañas
Instituto de Geología y Paleontología,
Vía Blanca, Línea del Ferrocarril s/n, San Miguel del Padrón,
Havana, Cuba

P. Alfonso (✉)
Departament d'Enginyeria Minera i Recursos Naturals,
Universitat Politècnica de Catalunya,
Av. de les Bases de Manresa,
08242 Manresa, Barcelona, Spain
e-mail: pura@emrn.upc.edu

J. C. Melgarejo · J. A. Proenza
Departament de Cristal·lografia, Mineralogia i Dipòsits Minerals,
Universitat de Barcelona,
c/ Martí i Franquès s/n,
08028 Barcelona, Spain

A. E. Fallick
Isotope Geosciences Unit, SUERC,
East Kilbride, Glasgow G75 0QF, UK

Introduction

The El Cobre deposit, 13 km NW from Santiago de Cuba, is located in the Sierra Maestra Paleogene volcanic arc of the southeastern part of Cuba, (Fig. 1) and is the oldest copper mine in America. The deposit was discovered in 1530 and mined by galleries in 1544 (Ansted 1856). During five centuries of activity, more than one million tons of ore with >14% Cu and more than two million tons of ore with >3% Cu have been extracted. During colonial times (up to 1898), galleries and mine shafts up to 300 m deep were developed on vein-type mineralisation. From the 1970s to the present, open pit mining has operated at the Mina Grande and Mina Blanca sectors, although the Cu vein mineralisation continues more than 1 km eastwards (Gitanilla sector). In the 1960s, a series of deep test drills towards the flanks of the deposit (Barita Occidental, Barita Oriental, Mina Nueva and Melgarejo sectors) led to the

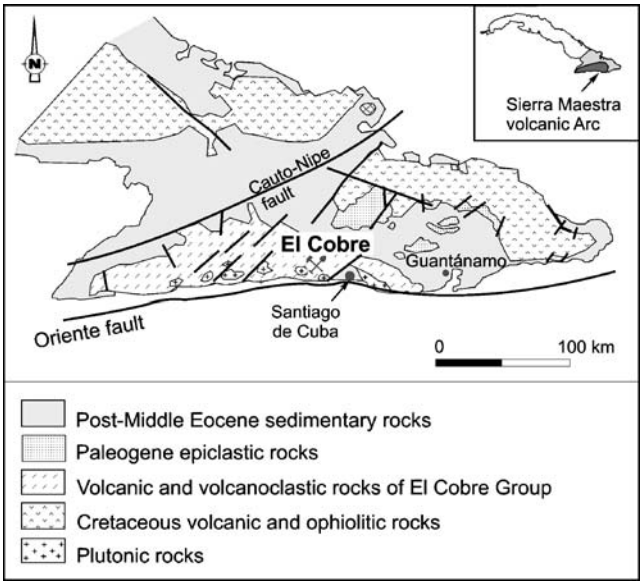

Fig. 1 Schematic geological map of the Sierra Maestra range showing the location of the El Cobre deposit (modified from Iturralde-Vinent 1996)

discovery of stratiform and stratabound polymetallic mineralisation (Cazañas et al. 1998), holding gold-bearing polymetallic ores with up to 25 ppm Au. In the 1990s these discoveries prompted foreign mining companies to investigate the new findings; in 1998, however, the copper mine was closed, despite known reserves of more than two million tons of ore with >1% Cu. At present, a new project for the evaluation of the flanks is being carried out by the Empresa Geominera Oriental from Santiago de Cuba.

In spite of the economic interest of this deposit, only a few published works are available, and most of them were part of studies of regional metallogeny (Kesler et al. 1990; Russell et al. 2000). Previously, the El Cobre deposit was attributed to a mesothermal origin (Cabrera et al. 1983) and an epithermal origin (Kesler et al. 1990). However, Cazañas et al. (1998), following a detailed structural investigation of the deposit, considered it to be a VHMS deposit; Russell et al. (2000) concurred.

This study presents detailed structural, mineralogical and textural data with a sulphur isotope and fluid inclusion study of the El Cobre deposit; the aim is to characterise the deposit and refine the genetic model of formation proposed in Cazañas et al. (1998).

Regional geology

The Sierra Maestra range formed as a result of the collision of the eastern Cuban microplate with the North American plate, with the development and activation of the North Caribbean transform fault, during the Oligocene. The North Caribbean transform fault was reactivated during the Miocene, modifying the overall structure of Sierra Maestra by wrenching and determining the present southern slope of the range (Rojas-Agramonte et al. 2005, 2006).

The Sierra Maestra is composed of a Cretaceous basement of arc-related rocks, unconformably overlain by widespread Paleogene volcanic arc rocks, which are overlain by Middle to Upper Eocene sedimentary rocks of the Puerto Boniato and San Luis Formation (Iturrale-Vinent 1996; Cazañas et al. 1998; Kysar 2001; Rojas-Agramonte et al. 2004, 2005, 2006) (Fig. 2). The Paleogene volcanic island arc, developed between the Paleocene (Thanetian) and the Early Middle Eocene, is represented by the El Cobre Group, a sequence of volcanic rocks more than 4,000 m thick (Iturralde-Vinent 1996, 1998; Cazañas et al. 1998; Rojas-Agramonte et al. 2006).

The El Cobre Group consists of volcanic and volcaniclastic rocks with intercalations of epiclastic material and fossiliferous limestones. The volcanic sequence is comprised of lavas, pyroclastic flows, subvolcanic sills and their feeder dykes (Iturralde-Vinent 1996; Cazañas et al. 1998; Kysar 2001; Rojas-Agramonte et al. 2006). The volcanic rocks in the lower and middle sequence of the El Cobre Group, in the Sierra Maestra range, are low-K island arc tholeiites (IAT), similar to those of the Kermadec arc in the SW Pacific (Cazañas et al. 1998; Kysar 2001; Rojas-Agramonte et al. 2006).

The Paleogene volcanic arc successions were intruded by calc-alkaline, low- to medium-K tonalites and trondhjemites during the final stages of subduction. These rocks have geochemical characteristics similar to subduction-related granitic rocks as found worldwide in intra-oceanic arcs (Kysar 2001; Rojas-Agramonte et al. 2004). Iturralde-Vinent (1996, 1998) considers that the El Cobre Group formed in the axial zone of the volcanic arc.

The El Cobre Group gives way by lateral facies change to the Pilón and Caney formations. It is divided into three sequences: lower, middle and upper (Méndez 1997) (Fig. 2). The lower sequence consists mainly of thick andesite–basalt flows, interbedded with several hundreds of metres-thick intermediate to basic tuffs. The middle sequence begins with andesite–dacite and conglomerates, giving way to several overlying cycles of explosive volcanism. Each cycle consists of pyroclastic deposits of coarse to very coarse grain size, indicating a proximal source. These deposits are followed by limestone olistostromes, which may be coeval with the emplacement of intermediate to acid lavas. The most important volcanic episode, 300 m thick, occurs close to the base of the sequence and consists of very coarse-grained pyroclastic rocks with fragments of more than 15 mm in diameter. This cycle is followed by another, 300 m thick, composed of finer-grained pyroclastic rocks with fragments up to 15 mm in diameter. At the top of this unit, limestone olistostromes

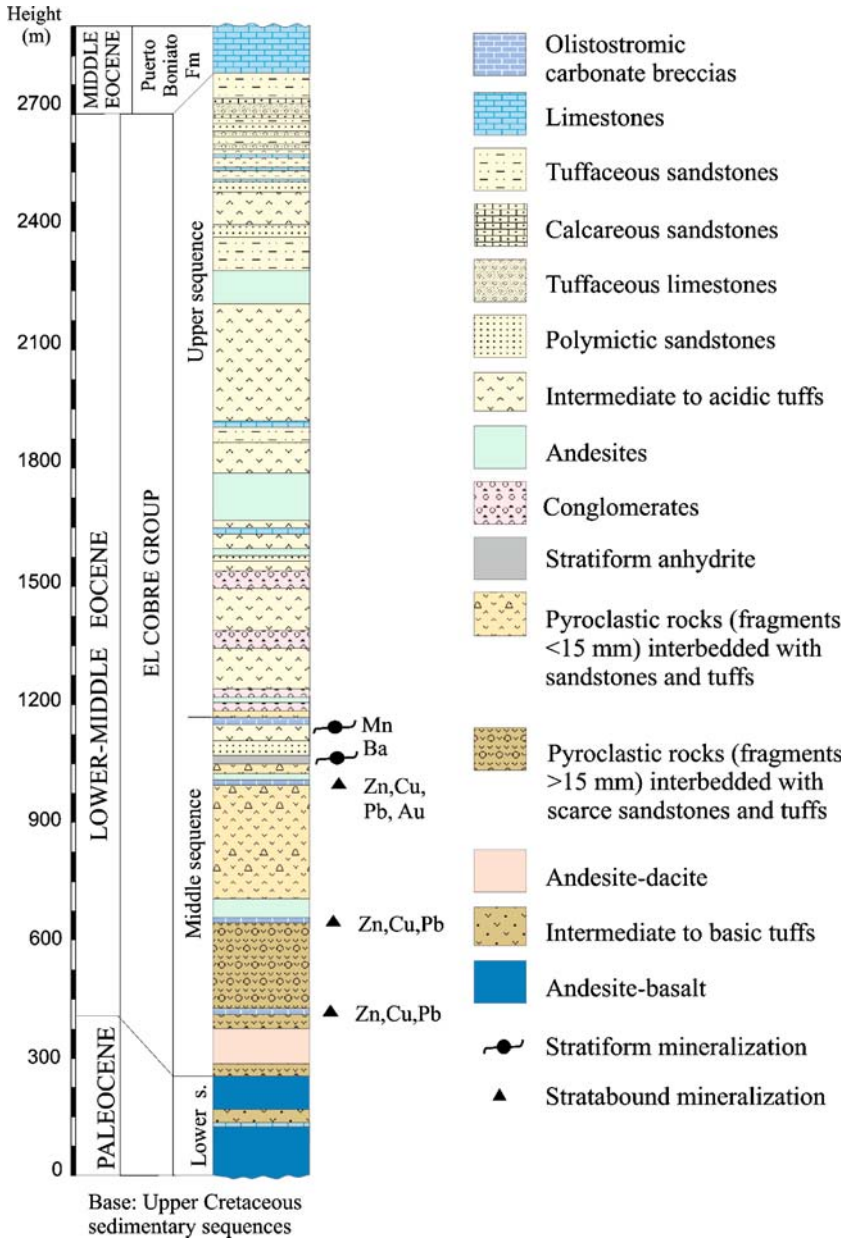

Fig. 2 Stratigraphic column of the Paleogene series in the easternmost part of Sierra Maestra through the El Cobre deposit (modified after Cazañas et al. 1998)

occur, and a stratiform mineralisation of anhydrite, barite and Mn oxides can be present. Most of the El Cobre deposit is hosted by rocks of the second cycle.

The contact between the upper and middle sequences is an unconformity. Thick conglomerate beds occur at the base of this sequence and vertically give way to other distal explosive volcanic cycles. In the El Cobre stratigraphic column, explosive cycles of the upper sequence consist of several tens of metres-thick beds of fine-grained breccias, followed by similarly thick beds of tuffs and ash tuffs located at the top. Epiclastic components and olistostromic limestones increase towards the top of the series, suggesting the progressive extinction of Paleogene volcanism and the subsequent dismantling of the volcanic structures.

Geology of the deposit

The ore deposit is hosted by volcaniclastic rocks of the Middle Sequence of the El Cobre Group, near the unconformity with the Upper Sequence, which consist of marine conglomerates and sandstones (Fig. 2).

The Middle Sequence in the El Cobre deposit consists of coarse-grained pyroclastic rocks. Metre-sized fragments are common at the base of the sequence, whilst the upper part consists of an interbedding of several decimetres-thick beds of ash tuffs, lapilli tuffs and fine- to medium-grained epiclastic rocks. The composition of the pyroclasts is variable, from andesite–dacitic at the base to rhyolitic at the top. Two discontinuous, olistostromic

reefal limestones, up to several tens of metres in thickness, occur interbedded with the pyroclastic rocks at the top of the sequence and could represent episodes of tectonic instability in the Eocene basin. Volcanic dykes of different sizes and compositions, ranging from andesite–basalt to rhyolite, crosscut the previous units.

The ore bodies are located along the El Cobre fault (Fig. 3). This fault, more than 40 km long, is linked with an E–W fault system that generated two sets of associated joints trending SW and NW. Rocks in the fault zone show cataclastic textures. Quartz veins, hydrothermal alteration of host rocks and a copper vein mineralisation are associated with the fault zone; a late andesite–basalt dyke also intruded along the fault and cuts the vein mineralisation. To the east, Middle Eocene limestones from Sierra de Boniato preserve this fault. Hence, the El Cobre fault and the accompanying systems formed during the early stages in the development of the volcanic arc (Pérez and García 1997) and facilitated the development of fissure volcanoes in later stages.

A late Eocene strike–slip N–S system (Pérez and García 1997; Rojas-Agramonte et al. 2005) produced movements

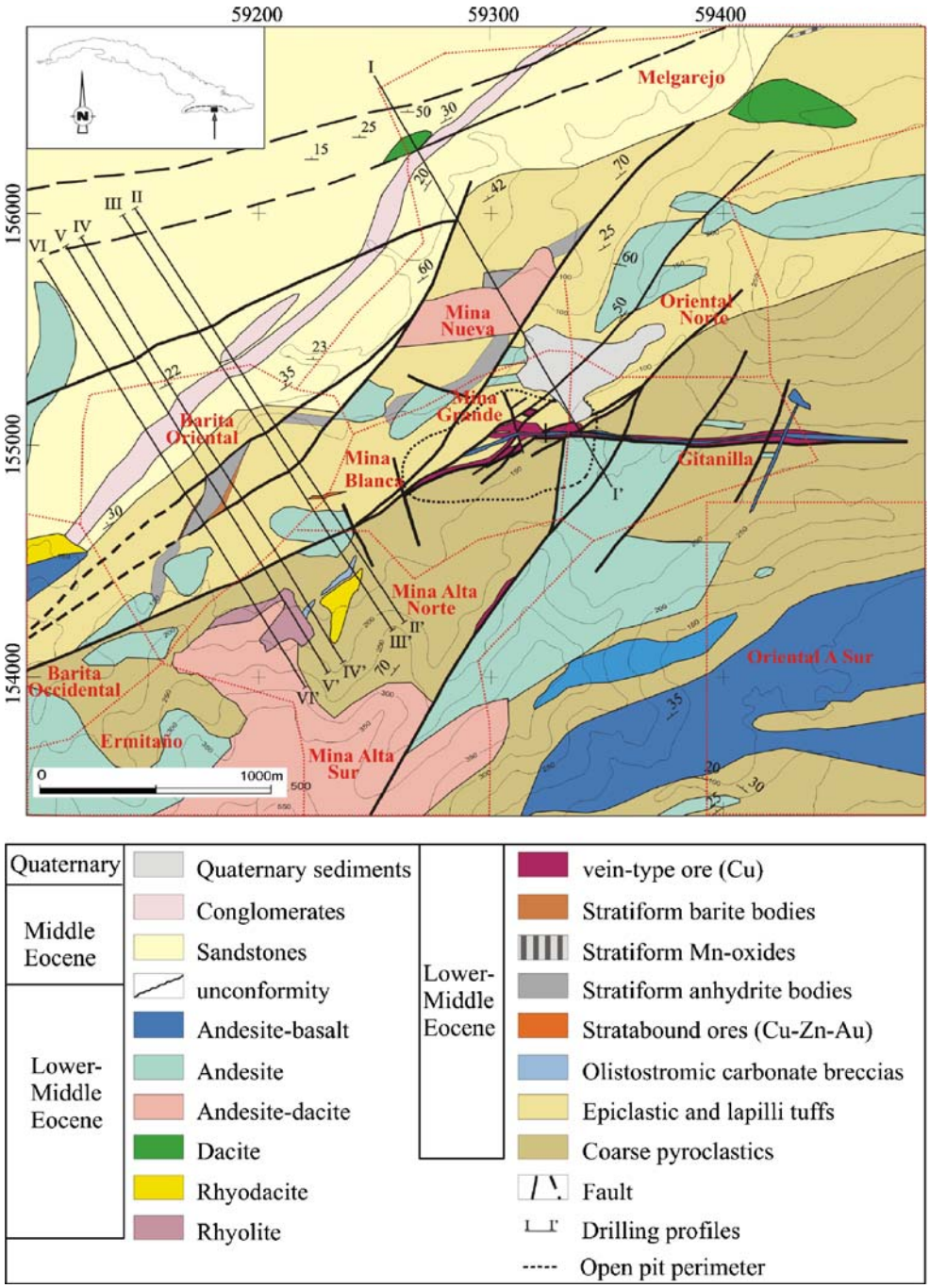

Fig. 3 Geological map of the El Cobre deposit (modified after Cazañas et al. 1998). The *straight transverse lines* indicate drilling profiles

of several tens of metres, developing a block structure to the deposit and tilting the blocks. Consequently, the present topographic height of the various outcrops differs from the original. These movements affected the thickness and concentration of ore bodies. The central sectors of the deposit, Mina Blanca and Mina Grande (Figs. 4 and 5), located in a raised block, display the maximum width, up to 24 m.

Mineralisation styles

Based on detailed drilling and the existing outcrops (Fig. 5), three main styles of mineralisation are distinguished in the El Cobre deposit: (1) stratiform (manganese, anhydrite and Au-bearing barite bodies); (2) disseminated, stratabound (polymetallic with Zn–Cu–Au); and (3) vein mineralisation, copper-rich with parallel veins at depth and stockwork development in surficial sectors.

Stratiform mineralisation

Stratiform lenses of manganese oxides, barite and anhydrite are located north of the El Cobre fault within an E–W trending belt. The lenses are typically about 1.7 km long and 100 m wide.

Stratiform Mn oxides These form a 4-m thick body which outcrops along more than 1 km in the north block of the El Cobre fault at a distal position. The base comprises an

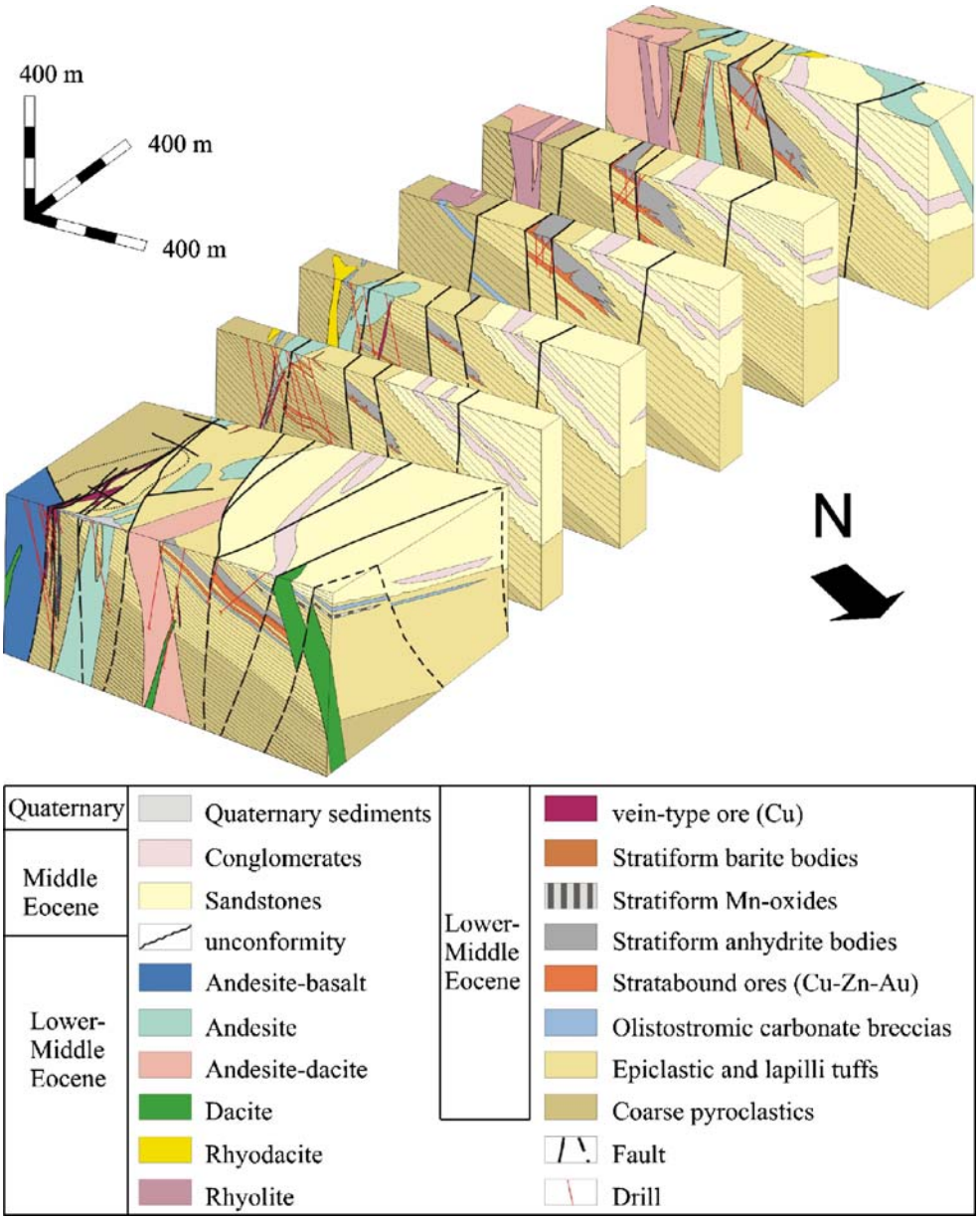

Fig. 4 Geological 3-D diagram compiled after drilling in the El Cobre deposit (see direction of the profiles in Fig. 3). Modified after Cazañas et al. (1998)

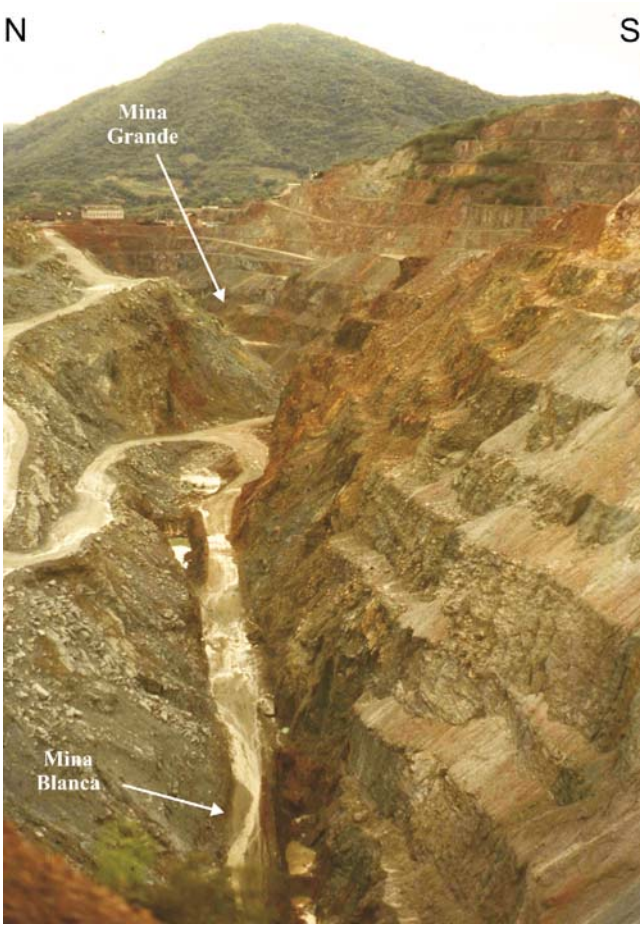

Fig. 5 General view of the El Cobre open pit

interbedding of red jaspers with scarce botryoidal cryptomelane and hematite beds up to 1.5 m thick in total, followed by a celadonite–hematite bed up to 1 m thick. A Mn-rich unit overlies this Fe-rich unit and consists of an interbedding of strata rich in Mn-silicates, mainly macfallite, chert and pyroclastic rocks cemented by cryptomelane. The top of the unit consists of 20 cm of massive cryptomelane.

Stratiform barite Two lenses of barite occur in the Barita and Melgarejo sectors. One, 4 m thick, is found at the footwall of the deposit and has nodular texture; it is crosscut by quartz–sericite–pyrite veins. The other, a 3-m thick lens, occurs at the hanging wall of the deposit and has massive or banded structure and foliated texture (Fig. 6a). These textures are similar to those reported in the Kuroko deposits in Japan (Shikazono 1994). Sphalerite, chalcopyrite and minor galena occur in the uppermost body, although euhedral or framboidal pyrite is the most abundant sulphide in this unit (Fig. 6b).

Stratiform anhydrite This unit, up to 100 m thick, consists of anhydrite beds interbedded with altered pyroclastic rocks. Anhydrite is bluish and has nodular texture (Fig. 6c). Nodules are regular or elongated, some millimetres to several centimetres in diameter. Near the base of the deposit, they are rimmed by euhedral quartz aggregates with montmorillonite and euhedral pyrite (Fig. 6d). In addition, a second replacement generation of fine-grained anhydrite occurs. All textural types of anhydrite are replaced by several generations of gypsum. Quartz and pyrite veins crosscut this unit; these veins are more frequent in the lower part.

Stratabound mineralisation

Three stratabound units can be distinguished according to depth: lower, intermediate and upper (Cazañas et al. 1998). The ores do not outcrop and were recognised by drilling. Quartz veins of variable thickness crosscut the stratabound mineralisation in the vicinity of the El Cobre fault; these veins can contain pyrite and chalcopyrite.

Lower stratabound mineralisation Five ore bodies, several tens of metres long and 4–8 m thick, occur in an area of 700×400 m in the west of the Mina Blanca sector. The mineralisation replaces olistostromic limestone bodies. There is a horizontal zoning related to the El Cobre fault. Highly recrystallised carbonate beds occur in the most distal zones, although micritic textures may also be preserved. Primary calcite is strongly replaced by bladed calcite, followed by sparitic calcite, sometimes with a phanerocrystalline talc+pyrite+chalcopyrite+quartz association.

In a more internal zone, anhydrite and quartz replace calcite. Anhydrite is, in turn, replaced by hematite, which is pseudomorphed by magnetite and, this, eventually, by pyrite. Quartz–chlorite–pyrite associations can pseudomorph anhydrite crystals.

Close to the El Cobre fault, the lower stratabound mineralisation consists of massive micro- to phanerocrystalline quartz aggregates associated with chalcopyrite, pyrite, minor amounts of sphalerite and Fe-rich chlorite. Kaolinite commonly occurs as inclusions within quartz. Minor amounts of hessite (Ag_2Te), tetradymite (Bi_2Te_2S) and tellurobismuthite (Bi_2Te_3) are associated with chalcopyrite.

Intermediate stratabound mineralisation This mineralisation is located several metres above the previous unit and comprises a partly silicified, discontinuous carbonate level of tens of metres in thickness. Zn–Pb sulphide mineralisation occurs in some areas.

Upper stratabound mineralisation This mineralisation comprises a polymetallic Zn–Cu–(Pb) layer, 1.7 km in length and

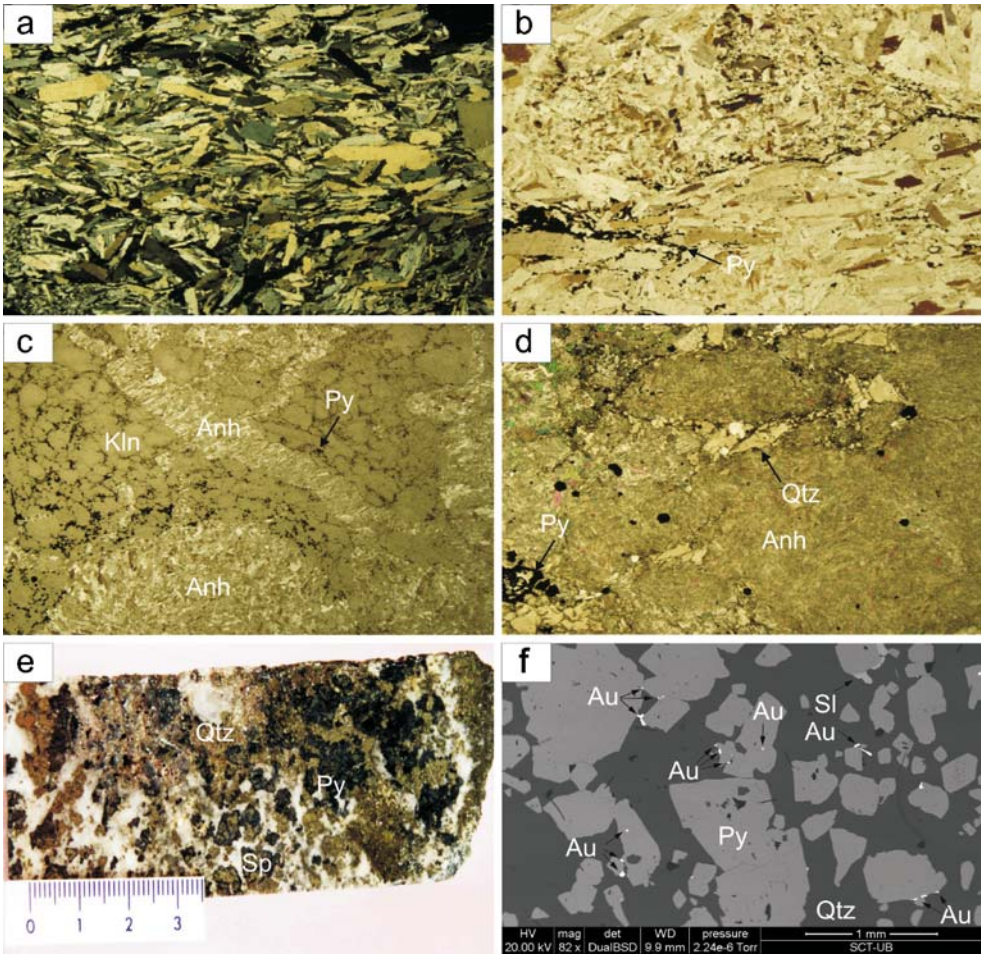

Fig. 6 Examples of textures of the stratiform and stratabound mineralisations: **a** foliated barite aggregates from the upper stratiform barite lens in cross-polarised light (width of image, 5.6 mm); **b** barite aggregates with fine-grained pyrite from the upper stratiform barite lens in parallel-polarised light (width of image, 5.6 mm); **c** anhydrite nodules and veins cutting across nodular kaolinite with pyrite in parallel-polarised light (width of image, 5.6 mm); **d** late quartz and pyrite crystals replacing anhydrite in the stratiform anhydrite lens in parallel-polarised light (width of image, 5.6 mm); **e** sphalerite and pyrite disseminated in quartz in the upper stratabound body; **f** SEM-BSE image of gold included into pyrite crystals from the upper stratabound body. *Py* pyrite, *Sp* sphalerite, *Anh* anhydrite, *Qtz* quartz, *Kln* kaolinite

90 m thick with low Cu/Zn ratio. This layer is located at the north of the El Cobre fault. It occurs directly below the anhydrite deposit near to the surface, but outcrops are scarce. According to texture, three zones can be distinguished within the body: (1) basal zone, (2) silicification zone and (3) contact zone with the upper anhydrite stratiform deposit.

In the contact zone with the host rock, microcrystalline quartz, montmorillonite, anatase, pyrite and other sulphides replace anhydrite. Pyrite is the most abundant sulphide; it becomes almost massive. Pyrite is usually corroded by sphalerite (I) and chalcopyrite. Sphalerite I is replaced by chalcopyrite and a late sphalerite generation (sphalerite II). Chalcopyrite locally co-crystallises with bornite and chalcocite, suggesting a high fugacity of sulphur.

The silicified zone consists of quartz with disseminations of chalcopyrite, sphalerite, pyrite and gold (Fig. 6e and f). Quartz, pyrite and sphalerite crystals contain remains of strongly corroded anhydrite crystals. Gold occurs interstitially among quartz grains or overgrowing early-formed pyrite crystals, and it is sometimes associated with hessite (Ag_2Te) and chalcopyrite in small veins that crosscut pyrite.

Therefore, this mineralisation can be interpreted as the replacement of the basal anhydrite bodies and volcanosedimentary rocks at the base of the stratiform deposit by a silicification process. The basal zone, roughly tabular and several metres thick, consists of strongly kaolinitised, sericitised and silicified volcanosedimentary rocks. It contains sphalerite, pyrite and chalcopyrite.

A mesh of veins, each up to several centimetres thick, cuts all the above-mentioned units. They are composed of vuggy quartz+chalcopyrite±sphalerite. Two types of sphalerite are present: a first generation (sphalerite I), strongly replaced by chalcopyrite, and a second generation (sphalerite II), that co-crystallises with chalcopyrite. Microcrystalline quartz constitutes a first generation of vein infilling; it is followed by a second generation of phanerocrystalline quartz, which contains abundant sericite inclusions. Radial kaolinite crystals coat the rhombohedral faces of these quartz crystals. On them, passive growths of pyrite and sphalerite II occur. This stage of mineralisation is rich in gold. Gold grains, more than 100 μm in size, occur associated with quartz or pyrite. Sphalerite II is sometimes slightly replaced by chalcopyrite. Galena, small native gold grains up to 10 μm in diameter, and calaverite ($AuTe_2$)

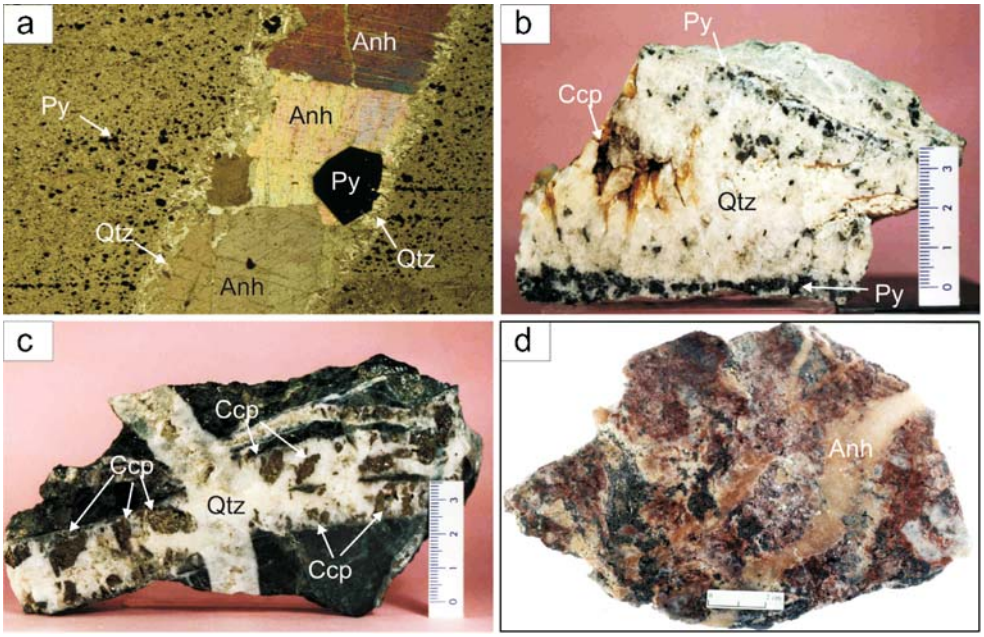

Fig. 7 Examples of textures of the stockworks: **a** quartz veins with chalcopyrite from the siliceous stockwork, Mina Grande; **b** detail of the internal banding in a quartz vein with sulfides from the siliceous stockwork, Mina Grande; **c** anhydrite veins cutting altered volcanic rock; **d** internal structure of an anhydrite–epidote vein with crystallisation of drusic quartz and pyrite crystals followed by anhydrite in parallel-polarised light (width of image, 5.6 mm). *Py* pyrite, *Ccp* chalcopyrite, *Qtz* quartz

rimmed by hessite, occur as inclusions in sphalerite II. A late vein stage consists of quartz, calcite and anhydrite, and they occur either as late discrete veins crosscutting the above-mentioned associations or as infillings of the vuggy porosity.

Vein mineralisation

Vein mineralisation in the Mina Blanca, Mina Grande, Mina Alta and Gitanilla sectors occurs along the El Cobre fault in an area about 1,200×140 m. Minimum known depths are 500 m in Mina Grande and Mina Blanca sectors and 200 m in the Gitanilla sector. In Mina Alta, 800 m SW of Mina Blanca, veins up to 2 m wide are located in an area 270 m long and 130 m deep. Mina Alta is located on a satellite fracture. All of them have Cu >0.7% ore.

Four subtypes of veining can be established according to structural and mineralogical criteria: siliceous stockwork, anhydrite stockwork, siliceous subparallel veins and anhydrite–epidote veins. Subparallel vein mineralisation has an approximate E–W or ENE–SSW trend and 80–85° S dip. It is from one to several tens of centimetres in thickness and several hundreds of metres in length. The mineralisation follows the fault trend, suggesting a strong structural control for these veins. The veins can be siliceous near the El Cobre fault and of anhydrite–epidote composition towards the flanks of the deposit. Subparallel veins grade upward to a siliceous stockwork with chalcopyrite and pyrite; in the transition zone, very wide high-grade veins are found. The stockwork extends several hundreds of metres and consists of veins, up to 1 m wide, of variable orientation, although the prevailing direction is the same as the fault.

Siliceous subparallel veins These veins comprise vuggy infillings of fine-grained quartz which grades to larger crystals rich in sericite or chlorite inclusions associated with sulphides. Quartz crystals are coated by sericite. The remaining porosity is filled by anhydrite or late-formed calcite. Towards the top of the subparallel veins, chalcopyrite occurs associated with small amounts of hessite (Ag_2Te), coloradoite (HgTe), tellurobismuthite (Te_2Bi_3) and tetradymite (Bi_2Te_2S).

Anhydrite–epidote veins The mineralogy of these veins consists of cryptocrystalline quartz, followed by microcrystalline quartz with chlorite, calcite and zoned epidote in radial aggregates. Epidote is occasionally found associated with pyrite, chalcopyrite and sphalerite. Anhydrite or a late generation of calcite fills the remaining vein porosity (Fig. 7a). Contacts among these minerals do not show evidence of replacement.

Siliceous stockwork Veins are composed of quartz accompanied by pyrite and chalcopyrite. Sulphide-rich quartz veins show a symmetric, some centimetres thick, banding of vuggy quartz growths associated with interstitial pyrite and chalcopyrite (Fig. 7b and c). At the top of the deposit, sericite growths on quartz crystals include remains of anhydrite, calcite, hematite and rutile. Sericite is corroded by kaolinite. At the innermost part of the vein, chalcopyrite and pyrite occur, and sometimes no vuggy porosity is present.

Anhydrite stockwork This outcrops only in the uppermost section of Mina Blanca and consists of a dense mesh of anhydrite veins (Fig. 7d), many being subhorizontal. The

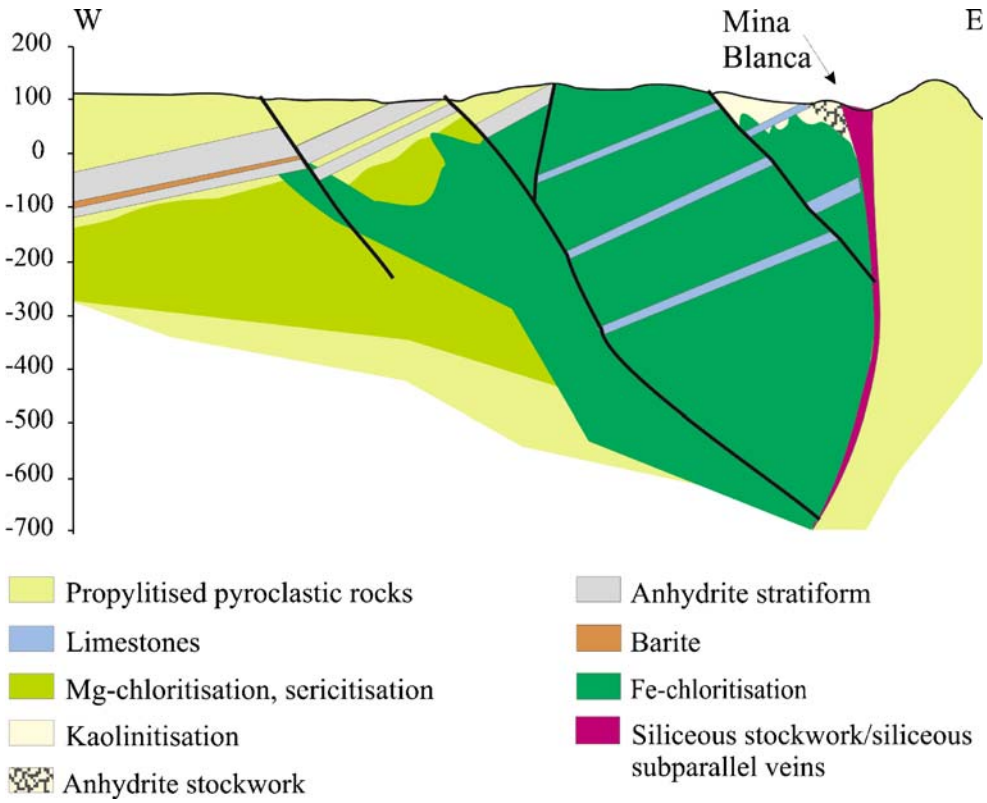

Fig. 8 Schematic profile of the El Cobre deposit where the strong alteration is shown

sequence of crystallisation in the veins starts with the development of calcite and anhydrite, together with lower contents of sphalerite and pyrite. These minerals infill all the vein cavity. A second silicification stage produces the replacement of anhydrite and calcite by quartz associated with small amounts of chlorite, apatite and pyrite.

Hydrothermal alteration

Significant hydrothermal alteration of the host rocks occurs in the proximity of the El Cobre fault; the distribution of the different alteration types is shown in Fig. 8.

The uppermost part of the deposit is strongly kaolinitised. This alteration develops around the anhydrite stockwork and especially inside the stratiform anhydrite and barite bodies. The replacement products consist of cryptocrystalline kaolinite and minor smectite.

Chloritisation, silicification and pyritisation are extensive close to the siliceous veins wherever they occur; similar hydrothermal alterations are found around the lower and intermediate stratabound bodies. Fine-grained chloritisation (Mg-rich chlorite) produces a complete replacement of the host rock. In turn, Mg-chlorite is replaced by Fe-rich chlorite, which is dominant in the uppermost part of the vein system. Pyritisation can be intense, and coarse pyrite crystals are formed in the replaced rocks. Silicification produces the development of small quartz veins and fine-grained quartz aggregates that can pseudomorph preexisting minerals in the volcanic host rocks. Sericitisation is poorly developed, and it only occurs around the uppermost part of the siliceous vein system. It is also accompanied by pyritisation and silicification.

A detailed study of these alterations in thin section identified the next stages of alteration, ordered from older to younger: kaolinitisation, chloritisation (Mg-rich)+pyritisation+silicification, chloritisation (Fe-rich)+pyritisation+silicification, sericitisation. By contrast, the volcanic rocks at the wall of the Mn stratiform mineralisation have green colour due to celadonite alterations.

Analytical methods

Based on the structural patterns described above, extensive sampling was undertaken to determine the conditions of formation of the deposit as elucidated by study of fluid inclusions and S isotopes.

Microthermometry of fluid inclusions was performed on 16 doubly polished thin sections using a Linkam THMSG 600 heating and freezing stage at the University of Barcelona. Calibration was made with standard compounds between −56.6°C and 263°C. The accuracy was ±0.2 for the final ice melting temperature and ±2.0 for the homogenisation temperature.

Table 1 Summary of microthermometric results of fluid inclusions from the different mineralisation styles of the El Cobre deposit

Style	Sample	Host mineral	*N*	T_h (°C) range	T_e (°C) range	T_{mice} (°C)	Salinity (wt% NaCl eq.)
S	S-69-183	Ba	19	185/291 (237)	−21/−22	−1.6/−2.4 (−1.9)	2.7/4.0 (3.3)
LS	488–310	Anh	6	196/222 (208)	−22	−2.9/−3.1 (−3.0)	4.7/5.1 (4.8)
LS	488–310	Cc	1	262	–	−3.5	5.7
IS	S-13a-190	Cc	38	150/216 (170)	−22/−22	−2.0/−3.7 (−2.8)	3.4/6.0 (4.7)
IS	S-39-285	Anh	5	178/226 (197)	−22	−2.1/−3.2 (−2.9)	3.6/5.3 (4.7)
US	S-42-141.3	Sph I	15	215/264 (243)	−21	−1.1/−1.7 (−1.3)	1.9/2.9 (2.3)
US	S-42-140	Sph II	26	217/268 (248)	−21/−22	−1.6/−2.5 (−1.9)	2.7/3.9 (3.2)
US	S-8-28	Sph II	20	189/245 (218)	−21/−22	−2.0/−3.1 (−2.3)	3.4/5.1 (3.9)
US	560–158	Sph II	8	173/277 (227)	−21/−22	−2.0/−2.4 (−2.1)	3.4/4.0 (3.6)
US	560–170.5	Sph II	12	176/259 (230)	−21/−22	−2.1/−3.0 (−2.4)	3.4/5.0 (4.4)
US	517–161	Sph II	1	214	–	−2.1	3.6
US	S-42-140	Qtz	2	207/230	–	−2.1	3.6
US	517–161	Qtz	1	225	–	−2.0	3.4
US	560–170.5	Anh	2	161/169	−22	−3.0/−3.3	5.0/5.4
FHS	S-76-158	Sph II	4	205/265 (247)	–	−2.2/−2.5 (−2.3)	3.7/4.2 (3.9)
AEV	S-76-158	Sph II	4	205/265 (247)	–	−2.3/−2.5 (−2.4)	3.9/4.2 (4.1)
AEV	S-32-344	Anh	6	157/190 (171)	−22/−23	−2.0/−2.2 (−2.1)	3.4/3.7 (3.5)
AEV	S-15-466	Anh	5	164/246 (206)	−22	−2.0/−2.9 (−2.4)	4.7/3.4 (4.0)
SS	32–27 S	Qtz	8	259/299 (279)	−21/−23	−1.9/−2.6 (−2.2)	3.2/4.3 (3.7)
SS	17-1	Qtz	24	263/293 (281)	−21/−22	−1.6/−2.3 (−2.0)	2.7/3.9 (3.4)

Average results are given in parentheses
S: stratiform, *LS*: lower stratabound, *IS*: intermediate stratabound, *US*: upper stratabound, *FHS*: siliceous subparallel veins, *AEV*: anhydrite–epidote veins, *SS*: siliceous stockwork, *N*: number of measurements, T_e: first melting temperature, T_{mice}: final ice melting temperature, T_h: homogenisation temperature

Raman spectroscopic analyses were carried out on representative fluid inclusions with an Yvon–Jobin Raman scanning spectrometer, operating with a 488-nm exciting frequency at a laser beam power of 600 mW. The presence of CO_2, H_2S, N_2 and CH_4 was investigated.

Sulphur isotopes were analysed in 24 samples of sulphates and 74 samples of sulphides representative of the different types of mineralisation: 22 analyses in chalcopyrite, 28 in pyrite, 23 in sphalerite and one in galena. Sulphates were mainly gypsum and anhydrite with two samples of barite. Minerals were separated by hand-picking techniques. Purity of the samples was tested by examination with a binocular microscope and X-ray diffraction. Individual crystals of different zones were selected for isotopic analyses in situ to determine the compositional variation at the crystal scale.

Analyses were performed at SUERC. Sulphates were treated using the method of Coleman and Moore (1978), and sulphides by that of Robinson and Kusakabe (1975); SO_2 was purified and subsequently analysed on a VG SIRA II mass spectrometer. In situ laser combustions were carried out with a Nd-YAG laser system following the method of Kelley and Fallick (1990), Fallick et al. (1992) and Hall et al. (1994). The results are given as $\delta^{34}S‰$ values relative to the V-CDT standard. The analytical precision is within ±0.2‰.

Fluid inclusions

Fluid inclusions are abundant in minerals from the different mineralisation units. All of them are two-phase, liquid–vapour. Only those classified as primary, according to the criteria of Roedder (1984) and Goldstein and Reynolds (1994), have been measured. Minerals used were quartz (stockwork and upper stratabound mineralisation), sphalerite (upper stratabound mineralisation and siliceous subparallel veins), anhydrite (upper, middle and lower stratabound mineralisation and anhydrite–epidote veins) and calcite (middle and lower stratabound mineralisation). The samples are representative of the different types of mineralisation except for the vein mineralisation where they belong to the most surficial parts because fluid inclusions from minerals of the lower zones are scarce and exhibit post-entrapment changes presumably acquired during recrystallisation.

Fluid inclusions occur isolated, following the crystal growth or in clusters located in the core of the crystal. The inclusions, up to 40 μm in size, are usually between 5 and 20 μm. The bubble occupies 10–20% of the total volume of the inclusion. Occasionally, trapped solids have been observed in quartz from the siliceous veins. Fluid inclusions with trails or necking down phenomena are common but only regular shape inclusions have been measured.

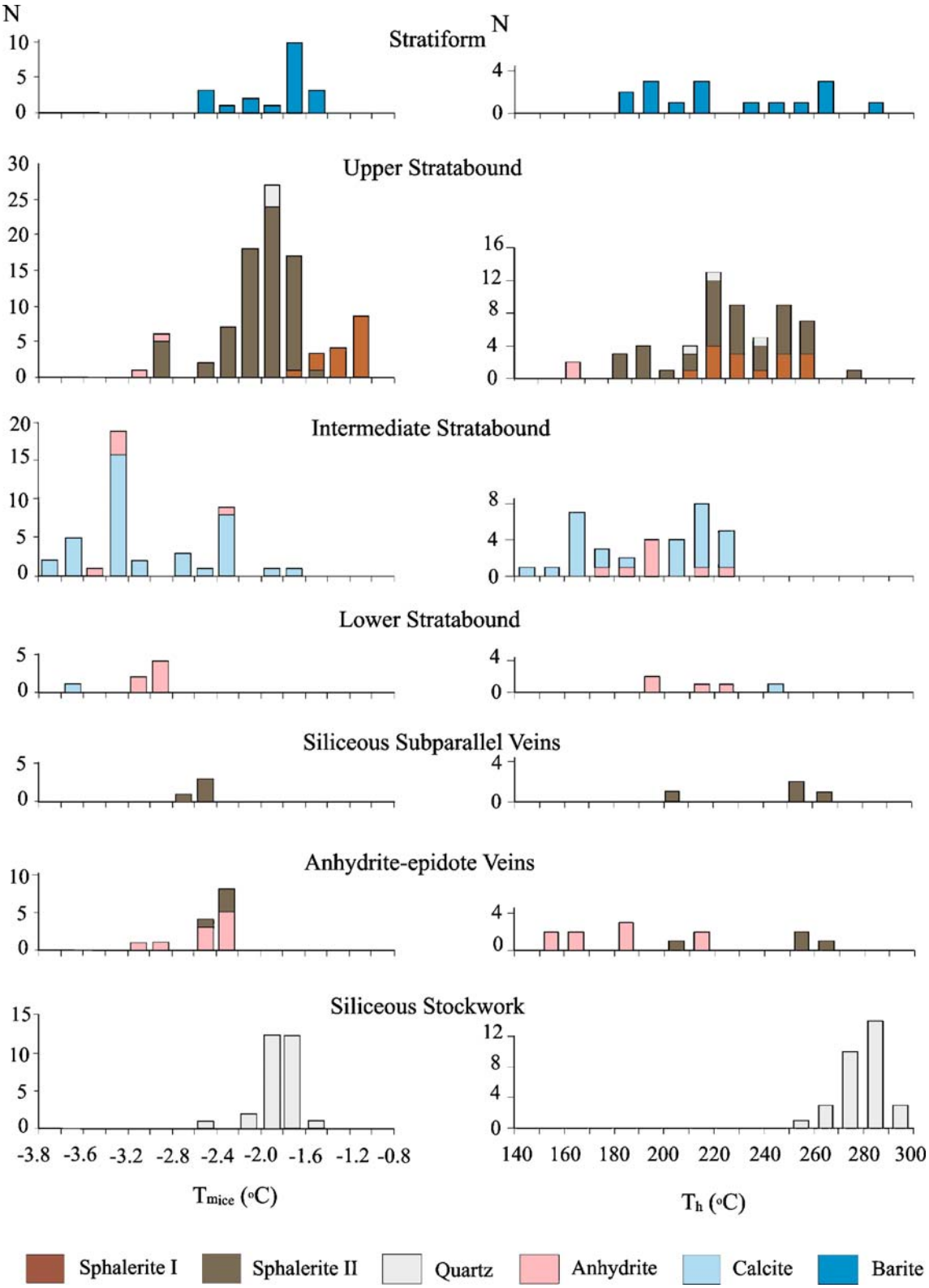

Fig. 9 Frequency histograms of the salinity and homogenisation temperatures of fluid inclusions from the different mineralisation styles of the El Cobre deposit

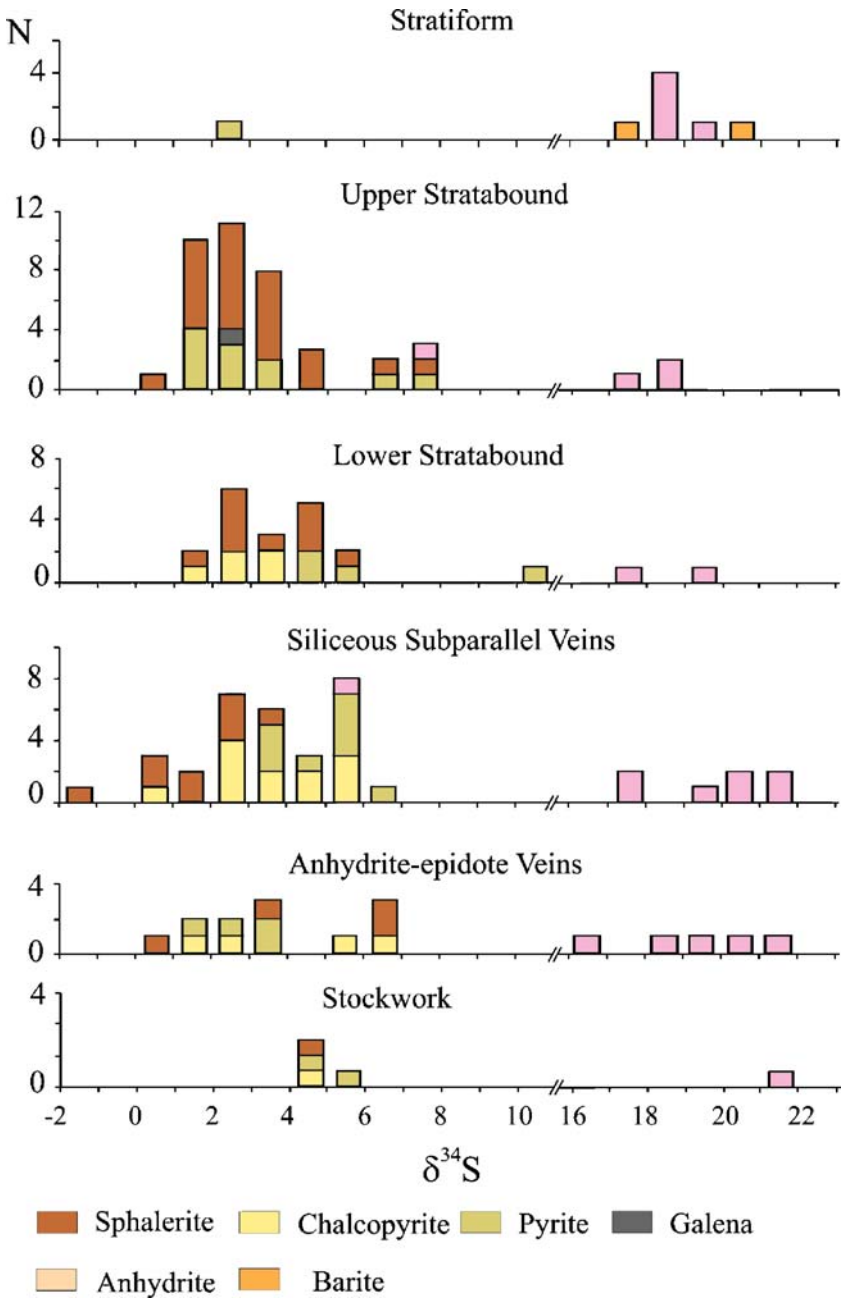

Fig. 10 Frequency histograms of $\delta^{34}S$ in sulphides and sulphates from the different styles of mineralisation from the El Cobre deposit

Table 1 and Fig. 9 summarise the microthermometric results of the fluid inclusions from the different minerals and units. The homogenisation is always to liquid, homogenisation temperatures ($T_{h(L-V)}$) range between 150°C and 300°C (Fig. 9). The highest temperatures belong to inclusions hosted within quartz from the siliceous stockwork (258–300°C), whereas calcite and anhydrite from the intermediate stratabound mineralisation exhibit the lowest homogenisation temperatures, between 150°C and 200°C. Early sphalerite (I) shows a narrow range of homogenisation temperatures, 243°C to 264°C (n=15), whereas late sphalerite (II) has a wide range, between 150°C and 268°C (n=82). Usually, inclusions in minerals from the stockwork and subparallel siliceous veins display higher homogenisation temperatures than those in minerals from the stratabound bodies; this is in agreement with the fact that these units represent the feeder zones of the deposit.

The temperature of first melting (T_e), between −22.5°C and −21°C, indicates that the dissolved salts are mainly NaCl (Potter et al. 1978). The temperature of ice melting, (T_{mice}), ranges between −3.7°C and −1.1°C. Clathrates have not been observed in any of the freezing runs. Raman spectrometry confirmed the absence of CO_2 and other volatile components in the fluid inclusions.

Salinities were calculated from the temperature of ice melting using the equation of Bodnar (1993), and they are

Table 2 Sulphur isotope composition ($\delta^{34}S_{CTD}$‰) for sulphides and sulphates from the El Cobre deposit

Sample	Style	Host rock	Ccp	Py	Sp	Gn	Anh	Brt	Sample	Style	Host rock	Ccp	Py	Sp	Anh
S-38-133	S	Anhydrite					18.3		488-310b	LS	Tuff			2.3	
S-38-138,9	S	Anhydrite					18.7		488-310c	LS	Tuff			2.6	
S38-142,5	S	Anhydrite					18.0		488-310d	LS	Tuff			2.1	
520-86	S	Gypsum					20.0		489-298	LS	Limestone			4.9	17.1
547-82,3	S	Gypsum		2.5					515-371	LS	Tuff	2.6			
564-56	S	Anhydrite				18.5		515-330	LS	Tuff	3.9		4.7		
S69-183,5	S	Barite					20.2	S-20-313,9	LS	Tuff	2.6	4.7			
S69-184	S	Barite					17.8	S30-370	LS	Tuff	1.9	10.6			
S-8-28a	US	Breccia			3.6				S-5-232	SSV	Tuff			1.2	
S-8-28b	US	Breccia			5.1				S-5-232	SSV	Tuff			2.7	
S-8-28b	US	Breccia			2.7				S-5-232	SSV	Tuff			1.4	
S-8-28b	US	Breccia			1.5				S-5-232	SSV	Tuff			2.5	
S-8-28b	US	Breccia			3.4				S13-222	SSV	Tuff			2.8	17.1
S-8-28b	US	Breccia			3.6				S13-222	SSV	Tuff				16.9
S-42-1	US	Breccia			2.5				S-15-438	SSV	Tuff		6.0		
S-42-1	US	Breccia			2.4				S19-50	SSV	Tuff	2.8	5.3		
S-42-1	US	Breccia			1.4				S19-53	SSV	Tuff		3.2		
S-42-1	US	Breccia			1.2				S-26-130	SSV	Tuff			3.8	
S-42-1	US	Breccia			2.1				S-47-193a	SSV	Andesite	6.0		1.5	5.7
S-42-136a	US	Breccia		1.8					S-47-193b	SSV	Andesite	5.6		-1.4	
S-42-136b	host rock	Breccia		7.6					S-47-194	SSV	Andesite				6.1
S-42-140	US	Breccia			3.5		19.0		S-47-194	SSV	Andesite			3.4	
517-53,3	US	Breccia		1.6	7.3	2.5	7.7		S-52-297	SSV	Tuff	4.3	5.4		
547-117	US	Breccia		6.5	4.7				S-76A-60,2	SSV	Breccia			2.9	
547-141,7	US	Breccia			4.0				P-23-12	SSV	Breccia	3.1			
560-153a	US	Breccia		3.5					308-3	SSV	Tuff	2.3			
560-153b	US	Breccia		2.5	6.0				381-47	SSV	Tuff	4.5	3.5		
560-165a	US	Breccia			2.5				383-165	SSV	Tuff	2.8			
560-165b	US	Breccia			2.5				383-174	SSV	Tuff	2.8			
560-165c	US	Breccia			5.0				384-244	SSV	Tuff				20.2
563-123	US	Breccia			4.5				384-245	SSV	Tuff				20.3
563-124	US	Breccia		5.6					463-233	SSV	Andesite	5.1	5.5		
563-125	US	Breccia							500-298	SSV	Tuff		5.7		
563-127	US	Breccia			3.8		19.5		482-501	SSV	Tuff	3.3	4.3		19.0
563-127b	US	Breccia			1.4				19-E	SSV	Breccia	0.9			
563-127b	US	Breccia			2.7				S10-716	AEV	Breccia	6.8			
563-127b	US	Breccia			1.5				S-15-466	AEV	Tuff				20.9
563-127b	US	Breccia		1.1	3.7				S-17-62a	AEV	Breccia		2.3		
563-127b	US	Breccia			3.6				S-17-62a	AEV	Breccia		3.7		
560-165b	US	Breccia			2.5				S-29-399	AEV	Tuff	1.1			
560-165c	US	Breccia			5.0				S-30-110	AEV	Tuff			3.1	
563-123	US	Breccia			4.5				S-32-344	AEV	Ash tuff		3.8		18.8
563-124	US	Breccia		5.6					S-32-409	AEV	Breccia			6.2	
563-125	US	Breccia							S-32-525a	AEV	Andesite	5.0	1.5		
563-127	US	Breccia			3.8		19.5		409-167	AEV	Breccia			0.8	20.0
481-296	LS	Breccia		4.3					485-221	AEV	Breccia			6.1	17.6
481-304	LS	Tuff	3.2				19.5		495-666	AEV	Rhyodacite	2.1			16.3
482-309	LS	Tuff		5.4	4.1										

Py: pyrite, *Sp*: sphalerite, *Ccp*: chalcopyrite, *Gn*: galena, *Anh*: anhydrite, *Brt*: barite, *S*: stratiform, *US*: upper stratabound, *LS*: lower stratabound, *SSV*: siliceous subparallel veins, *AEV*: anhydrite–epidote veins, *SS*: siliceous stockwork, *AS*: anhydrite stockwork

expressed as wt% NaCl equivalent. The range of salinity is between 1.9 and 6.0 wt% of NaCl eq. The lowest values of salinity belong to samples of early sphalerite I, highly replaced by chalcopyrite and barite. This sphalerite generation has a salinity range from 1.9 to 2.9 wt% NaCl eq., which is significantly lower than seawater salinity. Fluid inclusions from quartz have similar salinity to seawater, from 3.2 to 3.8 wt% NaCl eq. The highest salinity belongs to the fluid inclusions from the last minerals to be formed (anhydrite and calcite). Thus, fluid inclusions from El Cobre deposit indicate an increase of salinity with time.

Sulphur isotope data

Sulphur isotope results are listed in Table 2 and represented in Fig. 10. Sulphides from the feeder veins have δ^{34}S values between −1.4‰ and +6.8‰. δ^{34}S values in sulphides from the stratabound bodies range from 0‰ to +7.3‰, except one value of +10.6‰. Chalcopyrite from the feeder veins has δ^{34}S between +1.1‰ and +6.8‰, whilst for the stratabound bodies, δ^{34}S is between +1.9‰ and +3.7‰ (except one value of +5.1‰). Sphalerite from the subparallel veins has the lowest δ^{34}S values, between −1.4‰ and +3.8‰, whereas that located in distal positions (anhydrite–epidote veins) has δ^{34}S values up to +6.2‰. In the stratabound bodies, δ^{34}S varies between +3.3‰ and +7.3‰. Pyrite has a similar range of δ^{34}S in all the mineralisation (+1.5‰ to +6.5‰). The only δ^{34}S value measured on galena, located in the stratabound mineralisation, is +2.5‰.

The distribution of the isotopic composition of sulphur in the sulphides is not closely related with their distribution in the deposit, but there is a tendency for δ^{34}S to decrease with stratigraphic height and towards the most distal parts of the deposit.

Most sulphides exhibit an intra-grain zonation of the δ^{34}S values. Sphalerite from the stratiform bodies shows intra-grain variations of about 2‰. Usually, the lowest δ^{34}S values are in the core of grains and the highest in the rims (Fig. 11). Pyrite also shows a concentric zoning in δ^{34}S. Similar fluctuations in the δ^{34}S values where found in other VHMS deposits (Crowe et al. 1990; Crowe and Valley 1992; Sharp and Gemmell 2000).

The δ^{34}S values of sulphates (gypsum, anhydrite and barite) range from +16.3‰ to +20.9‰, except for two samples of anhydrite from the upper stratabound mineralisation and the subparallel veins with +7.7‰ and +5.9‰, respectively.

Discussion

Source of fluids

Most fluid inclusions from the El Cobre deposit exhibit similar or slightly higher salinity than that of seawater. Therefore, it can be assumed that seawater was the main fluid in the formation of the deposit; this is consistent with the paleoenvironmental conditions active during the deposition of the El Cobre Group (Kysar 2001) and its interbedded stratiform mineralisations.

Nevertheless, fluid inclusions from early sphalerite (I) have lower salinity with a mean of 2.3 wt% NaCl eq. Other VHMS deposits have those low values of salinity, mainly in sphalerite (Urabe and Sato 1978; Watanabe 1979, Bryndzia et al. 1983, Lüders et al. 2001; Ulrich et al. 2002). Possible explanations for such values are mixing of hydrothermal and meteoric fluids and a secondary origin of the inclusions (Pisutha-Arnond and Ohmoto 1983; Bryndzia et al. 1983; Ohmoto 1996) or a magmatic fluid input (e.g. de Ronde 1995). Meteoric fluids were unlikely to have been involved, taking into account the paleogeographic environment at the time of formation (Kysar 2001). Although a secondary origin for the inclusions cannot be absolutely ruled out, other possibilities should be taken into account.

A super-critical phase separation or boiling process is often suggested to explain low salinity in massive sulphide deposits. Phase separation can occur in two ways: (1) boiling of the hydrothermal fluids (Bischoff and Pitzer 1985; Rona 1988; Cathles 1993, Scotney et al. 2005) and (2) a separation of phases during the magmatic–hydrothermal transition. A contribution of volatile-rich magmatic fluids was suggested by different authors to explain the salinity of fluids in VHMS deposits (de Ronde 1995; Yang and Scott 1996; Scott et al. 1997; Herzig et al. 1998). Charlou et al. (1996) and Lécuyer et al. (1999) suggest that, after a volcanic eruption, two fluids can be exsolved: one dense, saline- and metal-rich and the other less dense with low salinity and volatile-rich. The model assumes the existence at a depth of magma in which

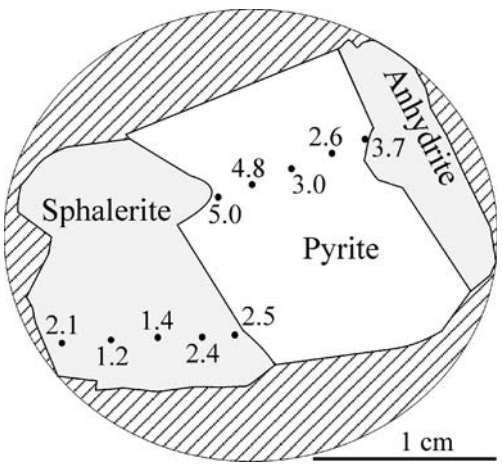

Fig. 11 Sketch showing the intra-grain sulphur isotope composition in a sample of sphalerite and pyrite from the upper stratabound mineralisation

exsolution produced two fluids: one vapour-rich and of low salinity and the other more saline. The difference in density causes the fluids to rise at different rates. Such unmixing phenomena are used to explain the formation of many deposits (Halter and Webster 2004).

Microthermometric results from fluid inclusions of the El Cobre deposit indicated that fluids involved in the formation of this deposit belong to the H_2O–NaCl system. In the El Cobre case, fluid inclusions do not show evidence of boiling. Homogenisation temperatures provide minimum estimated trapping temperatures. To determine the trapping temperatures, the pressure must be evaluated. In case of the absence of boiling, the minimum depth should be about 1 km. Moreover, the average of the present-day ocean depths at which anhydrite-bearing VHMS occur is between 1 and 2.5 km (Fouquet et al. 1993; Scott 1996; Fouquet 1997). Hence, taking into account this range of depths and a lithostatic pressure due to the anhydrite column of 100 m, the range of pressure at the top of the deposit should be between 138 and 270 bar. For such conditions of pressure, the correction of the homogenisation temperature to determine the temperature of entrapment is between 9°C and 15°C (Potter 1977). These data suggest that the deposit was formed within a range of temperatures from 175°C and more than 315°C.

Source of S

Sulphur in VHMS deposits usually comes from: (1) the inorganic reduction of seawater sulphate; (2) a magmatic source (Ohmoto 1996) that can result from a direct contribution from a vapour-rich magmatic fluid (Ohmoto 1986; Stanton 1990; Gemmell and Large 1992; Sillitoe et al. 1996, Herzig et al. 1998, Galley et al. 2000; Solomon et al. 2004) or (3) leaching of the volcanic host rocks (Solomon et al. 1988). Although the two magmatic sources produces a similar sulphur isotope composition, the direct magmatic contribution is more effective in the supply of metals, particularly Cu, Au, Bi and Te (Large 1992), and can be necessary to justify giant volcanogenic deposits (Ulrich et al. 2002).

Although sulphur from the bacteriogenic reduction of seawater sulphate has been considered important in some VHMS deposits (Sangster 1976; Çagatay and Eastoe 1995), the narrow range of $\delta^{34}S$ values observed in many VHMS deposits and the high temperature of formation are indicative of an inorganic reduction process of seawater sulphate (Sasaki and Kajiwara 1971). The inorganic reduction of seawater sulphate takes place easily in presence of ferrous iron when temperatures are above 250°C (Shanks et al. 1981; Shanks and Seyfried 1987). This process has been attributed to the presence of ferrous iron as reduction agent (Ohmoto et al. 1976; Ripley and Ohmoto 1977; Mottl et al. 1979; Shanks et al. 1981; Kerridge et al. 1983; Reed 1983). This origin has been considered for recent analogues to VHMS deposits (Arnold and Sheppard 1981; Styrt et al. 1981).

The relatively narrow range and positive $\delta^{34}S$ values of sulphides from the El Cobre deposit (−1.4‰ to +7.3‰) rules out a bacteriogenic source for the sulphur. This range is in agreement with sulphide derived from inorganic reduction of seawater sulphate, a process favoured by the high temperatures of the formation of the deposit and by the Fe-rich host rocks (Shanks et al. 1981; Shanks and Seyfried 1987). A similar origin has been considered for recent analogues to VHMS deposits (Arnold and Sheppard 1981; Styrt et al. 1981). The small variations in the sulphur isotopic composition of sulphides, sulphates (+16.3‰ to +20.9‰) and the intra-grain variations of the $\delta^{34}S$ values (up to 2‰) can be explained by the fractionation of sulphur isotopes during the thermochemical reduction of sulphate when seawater circulates deeply in a convective system.

However, a minor magmatic contribution of sulphide cannot be ruled out in interpreting these results. An important input of magmatic sulphur would produce negative $\delta^{34}S$ values as in the Hine Hina Mount (Herzig et al. 1998), yet these are not observed in the El Cobre case.

Most sulphates from El Cobre have $\delta^{34}S$ values (+16.3‰ to +20.9‰) similar to or slightly higher than Paleocene–Eocene seawater sulphate (+16‰ to +18‰; Claypool et al. 1980). These values indicate that sulphates were mostly formed from seawater sulphate and the higher $\delta^{34}S$ values could be due to minor contribution of hydrothermal sulphate, as occurs in other volcanic-hosted massive deposits (Ohmoto 1996; Solomon et al. 2004; Scotney et al. 2005). Two sulphate samples with very low $\delta^{34}S$ (+5.9‰ and +7.7‰) were likely formed from the oxidation of hydrothermal sulphide (Shanks and Seyfried 1987; Çagatay and Eastoe 1995; Lüders et al. 2001).

Genetic model

The El Cobre fault and its associated vein mineralisation, and the stratabound and stratiform ore mineralisations are clearly spatially related. Most of the mineralisation takes place in the footwall of the fault, which is in accordance with the synchronous character of both. Three stages are considered in the development of the El Cobre deposit (Fig. 12).

First stage of sulphate mineralisation

Similar to some modern VHMS (Laznicka 1988; Graham et al. 1988; Scott 1996; Lydon 1996; Herzig and Hannington 1995, Roberts et al. 2003; Bach et al. 2003), the El Cobre deposit contains a thick lens of anhydrite in its uppermost section, interbedded between two barite levels. The whole

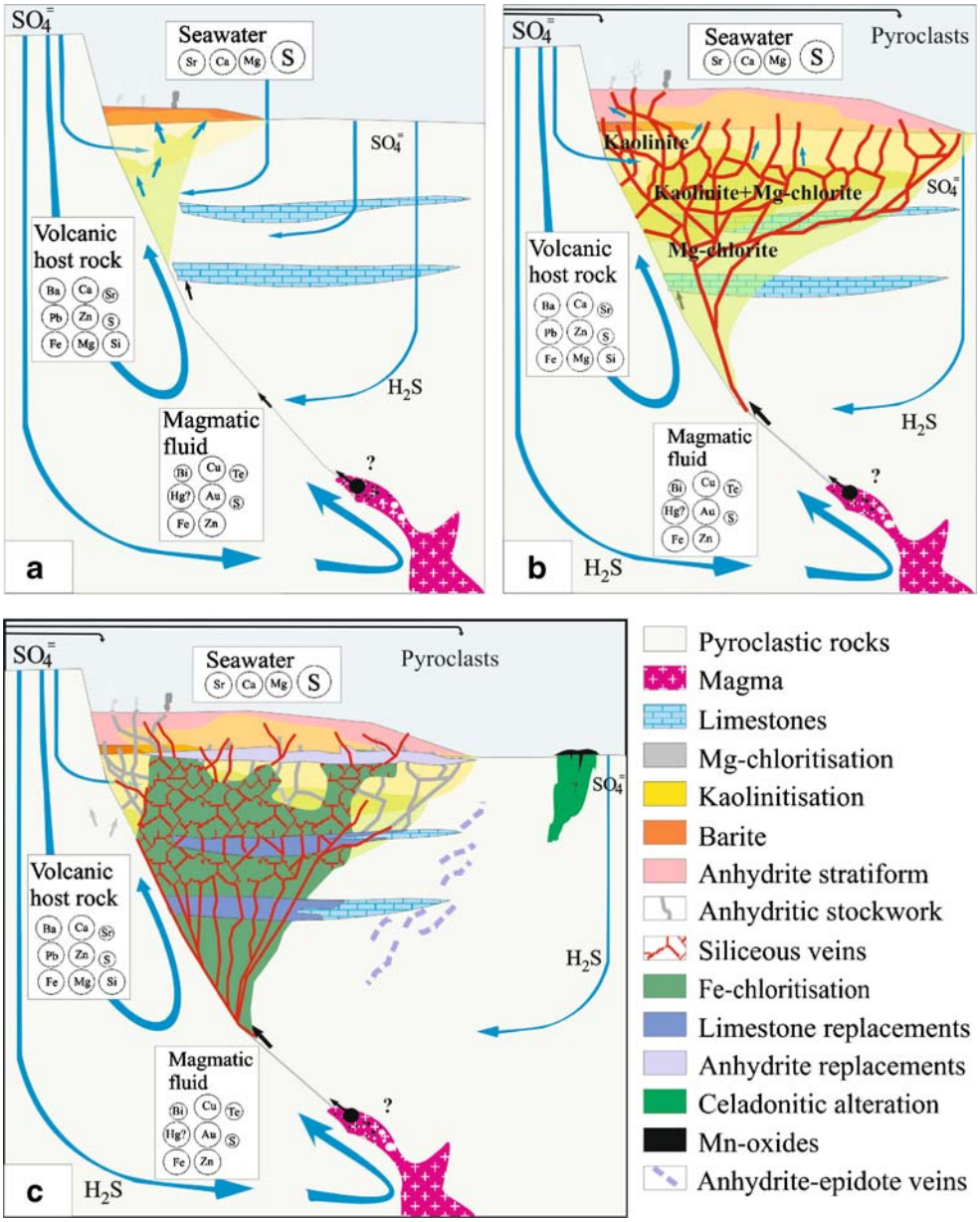

Fig. 12 Idealised representation of the stages of mineralisation in the formation of the El Cobre deposit showing the evolution of the ore mineralisation, alteration and the source of components. **a** Development of the stratiform barite lens; **b** development of the anhydritic stratiform mineralisation and the anhydrite stockwork; **c** development of the siliceous veins (stockwork and subparallel) and the stratabound mineralisations

is overlain by Mn oxide and chert stratiform deposits. A closely similar mineral association has been reported for VHMS deposits in Canada (Ridler 1971) and for several present-day VHMS deposits (Scott 1983, 1987, 1996). In this way, in the present-day Pacmanus hydrothermal system, exhalites formed from a hydrothermal plume of particles composed of anhydrite, barite, amorphous silica, metal sulphides, oxides and hydroxides (Scott et al. 1997). In addition, anhydrite and barite are important in the Kuroko deposits of Japan where the thickness of the bodies can achieve more than 100 m (Ogawa et al. 2007).

Textural and field evidence indicates that mineralisation begins with the precipitation of barite followed by kaolinite alteration and the deposition of anhydrite. Stratiform basal mineralisations of barite and anhydrite are very thick and massive with no petrographic evidence of formation from metasomatic replacement of other preexisting rocks. Moreover, sedimentary and diagenetic textures, nodules or lamination in anhydrite or barite deposits, exclude any replacement processes. The evaporitic origin of anhydrite is discarded for several reasons: (1) the sedimentary basin was deep submarine (Kysar 2001); (2) there are no remains of other evaporitic lithofacies and (3) no similar deposits occur in the rest of the Paleogene arc in Cuba. They are, therefore, chemical precipitates formed on the seafloor or in its vicinity; these sulphates formed through exhalative processes.

The occurrence of kaolinitic alteration in this stage indicates the acidic character of the solutions. Kaolinite occurs in various volcanogenic sulphide deposits where it is

associated with barite (Marumo 1989; Marumo and Hattori 1999; Petersen et al. 2002; Scotney et al. 2005). This acidity could be due to the contribution of a SO_2-rich magmatic fluid, which under cooling is decomposed into H_2SO_4 and H_2S (Herzig et al. 1998). This origin was proposed for kaolinite from high sulphidation epithermal deposits (White and Hedenquist 1995) and could be applied to VHMS deposits (Barrett et al. 2005). Thus, an early exsolved magmatic fluid could be mixed at depth with modified seawater, rise up along the El Cobre fault and other fractures and react with host rocks to form kaolinite.

Under the sulphate beds, a sulphate vein stockwork occurs. These veins can be interpreted as the root zone of an hydrothermal-exhalative sulphate deposit, as implied by: (1) both mineralisation styles coincide spatially; (2) absence of hydrothermal alteration to the top of the anhydrite unit similar to those found at the base of these bodies; (3) Cu ±Zn±Pb veins cut the base of anhydrite units but not its top and (4) vertical zoning of the vein mineralisation with transition from a siliceous stockwork zone to an anhydrite stockwork and, finally, stratiform sulphate mineralisation. Such zonal disposition can also be found in Kuroko-type deposits in Japan (Matsukama and Horikoshi 1970; Ohmoto and Skinner 1983), in VHMS deposits in Australia (Large 1992) and Canada (Roscoe 1965; Sangster 1976).

At this stage, the precipitation of sulphides was very low with some sphalerite and pyrite in the anhydrite stockwork. The precipitation of these sulphides might represent the mixing of cool seawater with the magmatic ascending fluid.

Second stage of mineralisation

Most of the sulphide mineralisation precipitated at this stage. This mineralisation fills all the channels and preexisting porosity and replaces previous mineralisation. The ore textures and the mineral composition of the alteration zones depend on the depth of formation.

The deep subparallel veins represent the feeder channels, which thin and converge at depth. These were formed at high temperature, around 300°C. In this study, there was relatively high tellurium abundance, and Au–Bi–Hg–tellurides were formed. The main source of fluid was modified seawater, which was the main source of sulphur, whilst the metals, as Cu, Bi, Au and Te, were probably mainly provided by a magmatic fluid, as occurs in other VHMS deposits (Large 1992), or leached from the host volcanic rocks (Huston et al. 2001).

The vertical zoning of the alteration with chlorite at its deeper sections, sericite and kaolinite at higher levels and talc at the top is characteristic of many massive sulphide deposits (Riverin and Hodgson 1980; Lydon and Galley 1986; Lydon 1996). This zoning can be considered a consequence of the thermal gradient established by the inflow of seawater from the surface.

Replacement zones or stratabound mineralisation are widely developed at this stage at the vicinity of the emission channels. Much of the previous mineralisation is replaced. The association quartz–illite–chlorite–apatite–sulphides of the anhydrite stockwork replaces that of calcite–anhydrite–kaolinite. Moreover, this association also replaces the stratiform barite and anhydrite mineralisations. The base of the anhydrite body is nearly completely replaced by aggregates of pyrite, chalcopyrite, sphalerite and bornite. The replacement of the anhydrite grains progress irregularly and usually it takes place in the intra-granular spaces of the anhydrite nodules.

In the stratabound mineralisation, carbonates are firstly replaced by an association of calcite+anhydrite and after, and especially near the El Cobre fault, by another of higher temperature, chalcopyrite+pyrite+sphalerite and silicification and pyritisation of the host rocks. Later, fracturing occurs in the upper stratabound mineralisation; the fractures are filled by siliceous mineralisation.

The El Cobre deposit zoning is characterised by a decrease in the chalcopyrite/sphalerite ratio towards the uppermost section and flanks of the deposit, as it draws further from its feeding zone. A similar zonation has been described by Lydon (1996) for VHMS and can be interpreted as a consequence of a thermal gradient during sulphide deposition. Chalcopyrite disease (Barton 1978) in sphalerite is abundant and occurs because of the replacement of sphalerite, formed at lower temperature, by chalcopyrite, formed at higher temperature.

Finally, anhydrite–epidote veins occur distally to the El Cobre fault and have been formed by the mixing of seawater and saline magmatic fluid; the temperatures were lower due to the distance from the higher temperature source.

Third stage of mineralisation

Finally, the development of barite at the top of the deposit and manganese mineralisation occurs. The occurrence of chalcopyrite and other sulphides with barite indicates that this mineralisation formed at relatively high temperature.

Conclusions

Based on the island arc geodynamic context in which it was formed, its localisation within a basaltic and andesitic submarine volcanic complex, its mineralogy, structure, texture and mineralogical zonation and sulphur isotopic composition the El Cobre can be considered to be a Cu–Zn–Pb sulphide volcanic-hosted deposit.

The ore mineralisation is the result of deposition from hydrothermal fluids circulating through the seafloor. These fluids produced three types of mineralisation: (1) vein mineralisation, formed by precipitation in feeder channels

with Cu at deeper levels and Zn at higher levels; (2) stratabound mineralisation with Zn–Cu–Pb–(Au), formed by partial replacement of some favourable levels (limestones at deeper levels and gypsum beds at the top of the sequence) and (3) stratiform anhydrite body at higher levels and stratiform mineralisation formed by exhalative processes at the Middle Eocene seafloor with anhydrite and barite at the base, barite towards the top and manganese bodies in distal position. As the deposit evolved, a telescoping effect was produced with low-temperature anhydrite stratiform deposits eventually being replaced and cut by new high-temperature vein generations.

The salinity of the fluid inclusions in the El Cobre deposit suggests that two fluids were involved in its formation: modified convective seawater and, to a lesser extent, a low salinity fluid, probably of magmatic origin. The sulphur isotopic composition of sulphides indicates that their source sulphur was mainly thermochemical reduction of seawater and, in minor amount, magmatic sulphur.

Although no stratiform sulphide mineralisation has been found, the existence of abundant replacement of anhydrite mineralisation by sulphide mineralisation suggests the possibility that these sulphides could have been formed in the previously eroded part of the deposit. Nevertheless, the occurrence of massive sulphide lenses at the anhydrite levels yet to be explored in the deposit must not be discarded, particularly, in the Melgarejo sector.

Acknowledgements This research was sponsored by a Ph.D. fellowship of the Agencia Española de Cooperación Iberoamericana (AECI) to X. Cazañas and by a postdoctoral fellowship of the Spanish Ministerio de Educación y Cultura to P. Alfonso. Additional funding was provided by grants to the authors from the AECI (Programas de Colaboración con Iberoamérica), from the Spanish project BTE2001-3308 and from the research grant 2005-SGR-00589 of the Departament d'Universitats, Recerca i Societat de la Informació (Generalitat de Catalunya). This paper is a contribution to the IGCP 502 "Global Comparison of Volcanic-hosted Massive Sulphide Districts". The mining companies Empresa Geominera de Oriente and JOUTEL provided samples and maps. The Fundació Solidaritat de la Universitat de Barcelona donated the heating/freezing stage to Instituto de Geología y Paleontología. SUERC is funded by NERC and the Scottish Universities Consortium. A. Tait is thanked for the support with the sulphur isotope analyses at SUERC and C. Ayora assisted with the fluids inclusion study. We thank Drs. Kerr and Roberts for their reviews, which have significantly improved the paper, and B. Lehmann for the editing.

References

Ansted DT (1856) The Cobre (copper) of Santiago de Cuba. Proc Geol Soc Lond 12:145–153

Arnold M, Sheppard SMF (1981) East Pacific Rise at latitude 21°N: isotopic composition and origin of the hydrothermal sulphur. Earth Planet Sci Lett 56:148–156

Bach W, Roberts S, Vanko DA, Binns RA, Yeats CJ, Craddock PR, Humphris SE (2003) Controls of fluid chemistry and complexation on rare-earth element contents of anhydrite from the Pacmanus subseafloor hydrothermal system, Manus Basin, Papua New Guinea. Miner Depos 38:916–935

Barrett TJ, MacLean WH, Aarebaeck H (2005) The Paleoproterozoic Kristineberg VMS deposit, Skellefte district, northern Sweden. Part II: chemostratigraphy and alteration. Miner Depos 40:368–395

Barton PB Jr (1978) Some ore textures involving sphalerite from the Furutobe mine, Akita Prefecture, Japan. Mining Geology 28:293–300

Bischoff JL, Pitzer KS (1985) Phase relations and adiabats in boiling seafloor geothermal systems. Earth Planet Sci Lett 75:327–338

Bodnar RJ (1993) Revised equation and table for determining the freezing point depression of H_2O-NaCl solutions. Geochim Cosmochim Acta 57:683–684

Bryndzia LT, Scott SD, Farr JE (1983) Mineralogy, geochemistry and mineral chemistry of siliceous ore and altered footwall rocks in the Uwamuki 2 and 4 deposits, Kosaka mine, Hokuroku district, Japan. Econ Geol Monogr 5:507–522

Cabrera R, Kramer JL, Pantaleón G (1983) Vinculación del magmatismo y los yacimientos meníferos de Cuba. Cienc Tierra Espac 9:47–56

Çagatay MN, Eastoe CJ (1995) A sulfur isotope study of volcanogenic massive sulfide deposits of the Eastern Black Sea province, Turkey. Miner Depos 30:55–66

Cathles LM (1993) A capless 350°C flow zone model to explain megaplumes, salinity variations, and high-temperature veins in ridge axis hydrothermal systems. Econ Geol 88:1975–1986

Cazañas X, Melgarejo JC, Luna A, Barrabí H (1998) El depósito volcanogénico de Cu–Zn–Pb–Au El Cobre, Cuba Oriental: estructura y mineralogía. Acta Geol Hisp 33:277–333

Charlou JL, Fouquet Y, Donval JP, Auzende JM, Jean-Baptiste P, Stievenard M, Mitchell S (1996) Mineral and gas chemistry of hydrothermal fluids on a ultrafast spreading ridge: East Pacific Rise, 17° to 19° S (Naudur cruise 1993). Phase separation controlled by volcanic and tectonic activity. J Geophys Res 101:15899–15919

Claypool GE, Holser WT, Kaplan IR, Sakai H, Zak I (1980) The age curves of sulphur and oxygen isotopes in marine sulphates and their mutual interpretation. Chem Geol 28:199–260

Coleman ML, Moore MP (1978) Direct reduction of sulfates to sulfur dioxide for isotope analysis. Anal Chem 50:1594–1595

Crowe DE, Valley JW (1992) Laser microprobe study of sulfur isotope variation in a sea-floor hydrothermal spire, axial sea mount, Juan de Fuca Ridge, Eastern Pacific. Chem Geol 101:63–70

Crowe DE, Valley JW, Baker KL (1990) Micro-analysis of sulfur-isotope ratios and zonation by laser microprobe. Geochim Cosmochim Acta 54:2075–2092

de Ronde CEJ (1995) Fluid chemistry and isotopic characteristics of seafloor hydrothermal systems and associated VMS deposits: potential for magmatic contributions. In: Thompson JFH (ed) Magmas, fluids and ore deposits. MAC Short Course Notes 23:519–527

Fallick AE, McConville P, Boyce AJ, Burgess P, Kelley SP (1992) Laser microprobe stable isotope measurements on geological materials: some experimental considerations (with special reference to $d^{34}S$ in sulphides). Chem Geol 101:53–61

Fouquet Y (1997) Where are the late hydrothermal sulphide deposits in the ocean? Philos Trans R Soc Lond 355:427–441

Fouquet Y, Von Stakelberg U, Charlou JL, Erzinger J, Foucher JP, Whitechurch H (1993) Metallogenesis in back-arc environments—the Lau basin example. Econ Geol 88:2150–2177

Galley AG, Van Breemen O, Franklin JM (2000) The relationship between intrusion-hosted Cu-Mo mineralisation and the VMS deposits of the Archean Sturgeon Lake mining camp, northwestern Ontario. Econ Geol 78:466–485

Gemmell JB, Large RR (1992) Stringer system and alteration zones underlying the Hellyer volcanic-hosted Massive sulfide deposit, Tasmania. Australia. Econ Geol 87:620–649

Goldstein RH, Reynolds TJ (1994) Systematics of fluid inclusions in diagenetic minerals. SEPM Short Course 31:199

Graham UM, Bluth GJ, Ohmoto H (1988) Sulfide-sulfate chimneys on the East Pacific Rise, 11° and 13° N latitudes. Part 1: mineralogy and paragenesis. Can Mineral 26:487–504

Hall AJ, McConville P, Boyce AJ, Fallick AE (1994) Sulphides with high: ^{34}S from the late Precambrian Bonahaven Dolomite, Argyll, Scotland. Mineral Mag 58:486–490

Halter WE, Webster JD (2004) The magmatic to hydrothermal transition and its bearing on ore forming systems. Chem Geol 210:1–6

Herzig PM, Hannington MD (1995) Polymetallic massive sulfides at the modern seafloor. A review. Ore Geol Rev 10:95–115

Herzig PM, Petersen S, Hannington MD (1998) Geochemistry and sulfur isotopic composition of the TAG hydrothermal mound, Mid-Atlantic Ridge, 26°N. Proc Ocean Drill Program Sci Results 158:47–68

Huston DL, Brauhart CW, Drieberg SL, Davidson GJ, Groves DI (2001) Metal leaching and inorganic sulfate reduction in volcanic-hosted massive sulfide mineral systems: evidence from the paleo-Archean Panorama district, Western Australia. Geology 29:687–690

Iturralde-Vinent MA (1996) Cuba: El archipielago volcánico Paleoceno-Eoceno medio. In: Iturralde-Vinent MA (ed) Cuban ophiolites and volcanic arcs. vol. 364. IGCP, Miami, FL, USA, pp 231–246

Iturralde-Vinent MA (1998) Sinopsis de la constitución geológica de Cuba. Acta Geol Hisp 33:9–56

Kelley SP, Fallick AE (1990) High precision spatially resolved analysis of $\delta^{34}S$ in sulphides using a laser extraction technique. Geochim Cosmochim Acta 54:883–888

Kerridge JF, Haymon RM, Kastner M (1983) Sulphur isotope systematics at 21°N site, East Pacific Rise. Earth Planet Sci Lett 66:91–100

Kesler SE, Levy E, Martín CF (1990) Metallogenic evolution of the Caribbean region. In: Dengo G, Case JE (eds) The geology of North America (vol. H: the Caribbean region). Geological Society of America, Boulder, CO, pp 459–482

Kysar G (2001) The role of Paleogene magmatism in the evolution of the northern Caribbean margin. The Sierra Maestra (southern Cuba). Unpublished Ph.D. Thesis. George Washington University, pp 187

Large RR (1992) Australian volcanic-hosted massive sulfide deposits: features, styles and genetic models. Econ Geol 87:471–510

Laznicka P (1988) Breccias and coarse fragmentites: petrology, environments, associations, ores. Elsevier, Amsterdam, p 832

Lécuyer C, Dubois M, Gruau G, Marignac Ch, Fouquet Y, Ramboz C (1999) Unmixing and seawater mixing in deep-sea hydrothermal systems: a microthermometric and oxygen isotope study of fluid inclusions in the baryte-sulfide chimneys of the Lau basin. J Geophys Res 104:17911–17929

Lüders V, Pracejus B, Hallbach O (2001) Fluid inclusion and sulfur isotope studies in probable modern analogue Kuroko-type ores from the Jade hydrothermal field (Central Okinawa Trough, Japan). Chem Geol 173:45–58

Lydon JW (1996) Characteristics of volcanogenic massive sulphide deposits: interpretations in terms of hydrothermal convection systems and magmatic hydrothermal systems. Bol Geol Min 107:215–264

Lydon JW, Galley A (1986) The chemical and mineralogical zonation of Mathiati alteration pipe, Cyprus, and genetic significance. In: Gallagher MJ, Ixer RA, Neary CR, Prichard HM (eds) Metallogeny of basic and ultrabasic rocks. Institution of Mining and Metallurgy, London, pp 49–68

Marumo K (1989) Genesis of kaolin minerals and pyrophyllite in Kuroko deposits of Japan: implications for the origin of hydrothermal fluids from mineralogical and stable isotope data. Geochim Cosmochim Acta 53:2915–2924

Marumo K, Hattori KH (1999) Seafloor hydrothermal clay alteration at jade in the back-arc Okinawa Trough: mineralogy, geochemistry and isotope characteristics. Geochim Cosmochim Acta 63:2785–2804

Matsukama T, Horikoshi E (1970) Kuroko deposits in Japan, a review. In: Tatsumi T (ed) Volcanism and ore genesis. University of Tokyo Press, Tokyo, pp 153–179

Méndez I (1997) Apuntes sobre el vulcanismo del Paleógeno en la región Sierra Maestra y características de su composición química. In: Furrazola G, Núnez K (eds) Estudios sobre Geología de Cuba. pp 424–444

Mottl MJ, Holland HD, Corr RF (1979) Chemical exchange during hydrothermal alteration of basalt by seawater—II. Experimental results for Fe, Mn and sulfur species. Geochim Cosmochim Acta 43:869–884

Ogawa Y, Shikazono N, Ishiyama D, Sato H, Mizuta T, Nakano T (2007) Mechanisms for anhydrite and gypsum formation in the Kuroko massive sulfide-sulfate deposits, north Japan. Miner Depos 42:219–233

Ohmoto H (1986) Stable isotope geochemistry of ore deposits. Rev Mineral Geochem 16:491–559

Ohmoto H (1996) Formation of volcanogenic massive sulfide deposits: the Kuroko perspective. Ore Geol Rev 16:135–177

Ohmoto H, Skinner BJ (1983) The Kuroko and related volcanogenic massive sulfide deposits: introduction and summary of new findings. Econ Geol Monogr 5:1–8

Ohmoto H, Cole DR, Mottl MJ (1976) Experimental basalt–seawater interaction: sulfur and oxygen isotope studies. EOS Trans Am Geophys Union 57:342

Pérez C, García D (1997) Tectónica de la Sierra Maestra (sureste de Cuba). In: Furrazola G, Núnez K (eds) Estudios sobre Geología de Cuba. pp 464–476

Petersen S, Herzig PM, Hannington MD, Jonasson IR, Arribas A Jr (2002) Submarine gold mineralization near Lihir Island, New Ireland fore-arc, Papua New Guinea. Econ Geol 97: 1795–1813

Pisutha-Arnond V, Ohmoto H (1983) Thermal history and chemical and isotopic compositions of the ore-forming fluids responsible for the Kuroko massive sulfide deposits in the Hokuroku district of Japan. Econ Geol Monogr 5:523–558

Potter RW (1977) Pressure corrections for fluid inclusion homogenisation temperatures based on the volumetric properties of the system NaCl–H_2O. J Res US Geol Surv 5:603–607

Potter RW, Clynne MA, Brown DL (1978) Freezing point depression of aqueous sodium chloride solutions. Econ Geol 73:284–285

Reed MH (1983) Seawater–basalt reaction and the origin of greenstones and related ore deposits. Econ Geol 78:466–485

Ridler RH (1971) Analysis of Archean volcanic basins in the Canadian shield using the exhalative concept. Can Min Metall Bull 64:20

Ripley EM, Ohmoto H (1977) Mineralogic, sulfur isotope, and fluid inclusion studies of the stratabound copper deposits at the Raul Mine, Peru. Econ Geol 72:1017–1041

Riverin G, Hodgson CJ (1980) Wall-rock alteration at the Millenbach Cu–Zn mine, Noranda, Quebec. Econ Geol 75:424–444

Roberts S, Bach W, Binns RA, Vanko DA, Yeats CJ, Teagle DAH, Blacklock K, Blusztajn JS, Boyce AJ, Cooper MJ, Holland N, McDonald B (2003) Contrasting evolution of hydrothermal fluids in the PACMANUS system, Manus Basin: the Sr and S isotope evidence. Geology 31:805–808

Robinson BW, Kusakabe M (1975) Quantitative preparation of sulfur dioxide for $^{34}S/^{32}S$ analysis from sulfdes by combustion with cuprous oxide. Anal Chem 47:1179–1181

Roedder E (1984) Fluid inclusions. Rev Miner 12:644

Rojas-Agramonte Y, Neubauer F, Kröner A, Wan YS, Liu DY, Garcia-Delgado DE, Handler R (2004) Geochemistry and age of late orogenic island arc granitoids in the Sierra Maestra, Cuba: evidence for subduction magmatism in the early Palaeogene. Chem Geol 213:307–324

Rojas-Agramonte Y, Neubauer F, Handler R, García-Delgado DE, Friedl G, Delgado-Damas R (2005) Variation of paleostress patterns along the Oriente Transform Fault, Cuba: significance for Neogene–Quaternary tectonics of the Caribbean realm. Tectonophysics 396:161–180

Rojas-Agramonte Y, Neubauer F, Bojar AV, Hejl E, Handler R, Garcia-Delgado DE (2006) Geology, age and tectonic evolution of the Sierra Maestra Mountains, southeastern Cuba. Geologica Acta 4:123–150

Rona PA (1988) Hydrothermal mineralisation at oceanic ridges. Can Mineral 26:431–465

Roscoe SM (1965) Geochemical and isotopic studies Noranda and Matagami areas. Trans Can Inst Min Metall Min Soc N S 68:279–285

Russell N, Moreira J, Sánchez R (2000) Volcanogenic massive sulphide deposits of Cuba. In: Sherlock R, Barsch R, Logan A (eds) VMS deposits of Latin America. Geol Assoc Can Spec Publ 2:241–258

Sangster DF (1976) Sulphur and lead isotopes in strata-bound deposits. In: Wolf KH (ed) Handbook of strata-bound and stratiform ore deposits. vol. 2. Elsevier, Amsterdam, pp 219–266

Sasaki A, Kajiwara Y (1971) Evidence of isotopic exchange between seawater sulphate and some syngenetic sulfide ores. Soc Mining Geol Japan Spec Issue 3:289–294

Scotney PM, Roberts S, Herrington RJ, Boyce AJ, Burgess AR (2005) The development of volcanic hosted massive sulfide and barite-gold orebodies on Wetar Island, Indonesia. Miner Depos 40:76–99

Scott SD (1983) Basalt and sediment hosted seafloor polymetallic sulfide deposits and their ancient analogues. Proc. Oceans'83. Marine Technology Society–Institute of Electrical and Electronic Engineers 2:818–824

Scott SD (1987) Seafloor polymetallic sulfides: scientific curiosities or mines of the future? In: Teleki PG, Dobson MR, Moore JR, Von Stackelberg JR (eds) Marine minerals: resource assessment strategies. NATO ASI Series C 194:277–300

Scott SD (1996) Short course: presently-forming hydrothermal deposits in the oceans and ancient ores on land. A comparison of modern and ancient massive sulfides and related deposits from a geological and geochemical point of view. Université de Bretagne Occidentale-Brest. Les Seminaires de L'École doctorale des Sciences de la Mer pp 39

Scott SD, Binns RA, Yang K (1997) Massive sulfide-forming systems on the present-day ocean floor. Proceedings of the Fourth Biennial SGA Meeting, Turku, Finland, pp 55–58

Shanks WC, Seyfried WE (1987) Stable isotope studies of vent and chimney minerals, Southern Juan de Fuca Ridge: sodium metasomatism and seawater reduction. J Geophys Res 92: 11387–11399

Shanks WC, Bischoff JL, Rosenbauer RJ (1981) Seawater sulfate reduction and sulfur isotope fractionation in basaltic systems: interaction of seawater with fayalite and magnetite at 200–350°C. Geochim Cosmochim Acta 45:1977–1995

Sharp R, Gemmell JB (2000) Sulfur isotope characteristics of the Archean Cu–Zn Gossan Hill VHMS deposit, Western Australia. Miner Depos 35:533–550

Shikazono N (1994) Precipitation mechanisms of barite in sulfate-sulfide deposits in back-arc basins. Geochim Cosmochim Acta 58:2203–2213

Sillitoe RH, Hannington MD, Thompson JFH (1996) High sulfidation deposits in the volcanogenic massive sulfide environment. Econ Geol 91:204–212

Solomon M, Eastoe CJ, Walshe JL, Green GR (1988) Mineral deposits and sulfur isotope abundances in the Mount Read volcanics between Que River and Mount Darwin, Tasmania. Econ Geol 83:1307–1328

Solomon M, Gemmell JB, Zaw K (2004) Nature and origin of the fluids responsible for forming the Hellyer Zn–Pb–Cu, volcanic-hosted massive sulphide deposit, Tasmania, using fluid inclusions, and stable and radiogenic isotopes. Ore Geol Rev 25:89–124

Stanton RL (1990) Magmatic evolution and the ore type-lava type affiliations of volcanic-exhalative ores. In: Hughes FE (ed) Geology of the mineral deposits of Australia and Papua New Guinea. Aus I M M Bull 14:101–108

Styrt MM, Brackmann AJ, Holland HD, Clark BC, Pisutha-Arnond V, Eldridge CS, Ohmoto H (1981) The mineralogy and the isotopic composition of sulfur in hydrothermal sulfide/sulfate deposits on the East Pacific Rise, 21°N latitude. Earth Planet Sci Lett 53:382–390

Ulrich T, Golding SD, Kamber BS, Zaw K, Taube A (2002) Different mineralisation styles in a volcanic-hosted ore deposit: the fluid and isotopic signatures of the Mt Morgan Au–Cu deposit, Australia. Ore Geol Rev 22:61–90

Urabe T, Sato T (1978) Kuroko deposits of the Kosaka mine, Northeast Honshu, Japan—products of submarine hot springs on Miocene seafloor. Econ Geol 73:164–179

Watanabe T (1979) Fluid inclusions in some Neogene ore deposits in the Green Tuff region, Japan. Mining Geology 29:307–321

White NC, Hedenquist JW (1995) Epithermal gold deposits: styles, characteristics and exploration. SEG Newsletter 23:1–14

Yang K, Scott SD (1996) Possible contribution of a metal-rich magmatic fluid to a seafloor hydrothermal system. Nature 383:420–423